Stony Brook University

Surface Damage Detection of CFRP Laminates Using Inverse Analysis

A Thesis Presented

by

Chong Huang

to

The Graduate School

in Partial Fulfillment of the

Requirements

for the Degree of

Master of Science

in

Mechanical Engineering

Stony Brook University

August 2009

Stony Brook University

The Graduate School

Chong Huang

We, the thesis committee for the above candidate for the

Master of Science degree, hereby recommend

acceptance of this thesis.

Toshio Nakamura – Thesis Advisor
Professor – Department of Mechanical Engineering

Chad Korach – Chairperson of Defense
Assistant Professor – Department of Mechanical Engineering

Robert Kukta – Member
Associate Professor – Department of Mechanical Engineering

This thesis is accepted by the Graduate School

Lawrence Martin
Dean of the Graduate School

Abstract of the Thesis

Surface Damage Detection of CFRP Laminates Using Inverse Analysis

by

Chong Huang

Master of Science

In

Mechanical Engineering

Stony Brook University

2009

Carbon fiber reinforced polymer (CFRP) laminated structures are very effective for weight saving in aerospace structural components. However, the damage of the material, like fiber breakages, fiber-matrix debonding, delamination and surface damage, will significantly influence the material stiffness. Surface damage can be caused due to high velocity impacts and it will significantly weaken material compression strength. The aim of the present work is to develop a novel method with the aid of an intelligent post-processing scheme so as to identify surface damage of CFRP. Due to the electrical properties of carbon fiber, a combination of electrical resistance change method (ERCM) and electrical potential change method (EPCM) is applied here as the basic approach to obtain necessary data. In the present verification and simulation analyses, a 2D CFRP laminates sample will first be introduced as the model to approve this procedure. Electrical potentials on discrete locations on the top of the sample are adopted as the input measurements. Though reasonable estimates are obtained with these measurements, additional improvements by adding an electrical resistance is applied in order to increase the accuracy. A detailed error sensitivity analysis is also carried out to confirm the robustness. Then the 3D situation is extended for further verification by applying almost

same procedure as 2D situation. The results suggest the current method can be an alternative approach to detect surface damage contained in CFRP laminates. Based on this analysis, proper electrode arrangement patterns are then proposed and experimented to see if accurate surface damage in real composites could be obtained. By comparison with the estimation accuracy of each pattern, "Square 0^{o}" pattern is considered to be a suitable one and the best electrode interval space is also defined. Furthermore, the depth of surface damage is also concerned unknown. Inverse procedure and error sensitivity analysis are performed again to estimate the four unknown parameters.

To my parents and friends

For their supports

Table of Contents

List of Tables

List of Figures

Acknowledgements

The two years' study experience in pursuing a master degree of mechanical engineering is wonderful and memorable for me. I am deeply grateful to my advisor, Professor Toshio Nakamura. Thanks to him, I get a brand new view of science and research work. His broad knowledge and passion toward scientific research encourage me to devote myself to the study of solid mechanics. Besides my advisor, I also want to thank the rest of my thesis committee, Professor Chad Korach and Professor Robert Kukta, who gave me insightful comments and reviewed my work on a very shot of notice. I should give my special thanks to my friend, Xi Yang, who gave me much useful advice during the research procedure. I would also like to thank all the faculty and staff in the Department of Mechanical Engineering, for their help with my studies.

I am indebted to my senior colleagues: Dr. Nanayanan Ramanujam, Jian Yao, Wei Zhao, for their generous help. I also want to thank all my fellow group colleagues: Yu Chen, Shu Guo, Zhiwei Shi and many others, for their care, support and friendship.

Last but not the least, I want to thank my parents, for their loving, supporting, concerning and understanding during my graduate study. This thesis is dedicated to them.

To all of you, thank you.

1. Introduction

Carbon fiber reinforced polymer (CFRP) laminate is being increasingly applied to the primary structure of aircraft, due to its high specific strength and stiffness. However, when the laminate is impacted by foreign objects, it is easy to be impaired, resulting in a reduction of the compression strength. If it is used as a structural component, it will become a problem to maintain the structural reliability. Aymerich et al. [1] characterized various damage types such as delamination between layers, matrix crack, and surface damage based on different impact situations. Schubel et al. [2] studied residual mechanical properties of a sandwich structure (core sandwiched in between face sheets) subjected to low velocity impact and found delamination in upper face sheets and indentation impressions in the contact area. Oka et al. [3] proposed a general damage predictive equation for any impact conditions and any material.

Commonly, non-destructive evaluation (NDE) techniques such as ultrasonic inspection, vibration response, infrared thermal images, and eddy current test are used to detect damage defects. For example, Aymerich and Meili [4] performed an ultrasonic inspection to detect delamination and they also discussed the combination of normal and oblique incidence pulse-echo ultrasonic techniques. Mool et al. [5] took the eddy current test to detect delamination with special probes. However, these conventional monitoring methods are very costly and time-consuming, and it is difficult to perform real-time monitoring. Therefore, a simple structural health monitoring method is urgently required to maintain structural reliability and reduce huge periodic inspection costs.

Since CFRP laminate consists of electroconductive carbon fibers and insulative resin, it is inhomogeneous material with strongly anisotropic electrical property. The electric potential technique can also be applied to CFRP laminate. However, electric current path may be complicated in the laminate due to the strong anisotropy. Electrical conductivities of CFRP can not be easily obtained because of the complex structure of the composite. Taking FE method as the artifice to measure the orthotropic electric conductance of CFRP laminates, Todoroki and Tanaka [6] obtained the detailed conductivities of CFRP for specific fiber volume values.

Flaw configurations in the laminate are different from those in metallic material. The electric potential technique must be developed to apply to CFRP laminate. Electric current also plays an important role when to measure electric resistance change between electrodes. The electrical potential change method (EPCM) and electrical resistance change method (ERCM) are both widely used for damage detection on CFRP research. Masahito et al. [7] used EPCM to detect the delamination location and size contained in the 2D CFRP model. Effect of spacing between electrodes was also studied using ERCM to monitor delamination for the same model [8]. Todoroki group also developed detailed research of damages in CFRP using this NDE technique, not only for delamination, but also for other damage types like matrix crack and so on [6-12]. The research group of Chung [13-14] used circumferential lead wires with silver paste as probes for the unidirectional CFRP laminated specimen to apply the electric current. ERCM was also applied to fatigue damage detection by many other researchers [15, 19-21].

The main goal of this study is to explore a detection method using EPCM and ERCM to offer robust surface damage identification. An efficient inverse method that post-processes the limited measured record is proposed. Recently, inverse analysis approaches are being increasingly implemented in mechanical problems. For example, Frederiksen [16] proposed an inverse approach for the identification of elastic properties of orthotropic plates. Moreover, various inverse analysis based techniques was applied to detect delamination type flaws. Liu and Chen [17] used an inverse technique to identify the presence, location and orientation of flaw in the core layer of sandwiched plates. Ishak et al. [18] showed an adaptive multi-layer perceptron (MLP) network for inverse identification of interfacial delaminations in carbon/epoxy laminated composite beams.

When complex materials such as composites are inspected, it is essential to have an intelligent process to filter out critical information from available measurement. The proposed inverse method is designed to process those measurements that do not relate directly to the unknown parameters. Here the unknown damage parameters are the location and size of the surface damage while the indirect measurements were chosen as electrical potential and resistance values. The detailed description of the procedure is explained next.

2. Identification of damage in CFRP laminates

Physical responses of some complicated systems sometimes cannot be directly obtained or measured. However, if they are dependent on some observable parameters, they can be estimated by using inverse analysis approach. Inverse analysis approach is used to connect such indirect measurements to the unknown parameters and since there are various inverse analysis methods, it is critical to establish a suitable model for given conditions.

In the current work, the unknowns are location and size of surface damage contained in the sample. Measurement values used for analysis are the electrical potentials on some appropriate locations and also the electrical resistance values between some reference points. An error object function is then formulated to examine the accuracy of estimates. Though various error object functions can be applied in this procedure, a good error object function usually could lead to precise estimation while a bad one may result in very rough solutions. At last, an inverse procedure is carried out to find the unknown parameters that yield to the lowest error object value by downhill simplex method, which is a multi-dimensional minimization algorithm. The details of the downhill simplex method are described in section 2.4.

2.1 Description of simulation process

In order to verify the procedure, a 2D CFRP sample is created with its size shown in figure 1. The sample is a four-ply $[0/90]_s$ composite laminate with surface damage located on the bottom layer. To make things easier, the depth of the damage is assumed to be a constant and it is set be equal to half layer thickness. Thus, to define a certain surface damage, only two variables, the location s and the size d, are required. Here, the surface damage location is measured from the middle of the damage to the left edge of the sample. Electrodes made with copper are mounted on the top layer of the sample for measurement of electrical potentials. In computational simulation, electrodes will not introduce any error, however, when mounting the electrodes on the sample in real experiment, good contact between electrodes and the CFRP sample is very important since weak contact could bring large error.

Surface damage will influence the electrical potential distribution and also the electrical current flux in the sample compare to a sample without any damage applying an exactly same boundary condition. However, for a region on the sample which is far enough from the location of the surface damage, the influence is small. Taking this into account, electrodes should be distributed fully and evenly on the top of the sample. In figure 1, electrodes A and B are current electrodes while electrodes 1-7 are voltage electrodes. Electrical potential values V_1-V_7 corresponding to electrodes 1-7 are measured to be the reference measurements.

The thickness of the sample is denoted as t = 1mm while the length is set as l (= 250t). In each ply, the material is assumed to be transversely isotropic and the electrical conductivities of the copper and CFRP are listed in table 1. As a composite material, CFRP has different electrical properties for different fiber volume fractions. Here, the electrical conductivities of CFRP when the fiber volume fraction is 60% are used [6]. The conductivities for fiber direction, transverse direction and thickness direction are denoted as σ_0, σ_{90} and σ_T. Before dealing with the inverse analysis procedure, the forward procedure should first be carried out to get the relationship between the surface damage and the reference values, V_1-V_7, respectively. For the whole procedure, the location and size of the surface damage are set in a domain. The location s ranges from 50mm to 200mm, and the size d ranges from 4mm to 40mm. The real relation between the surface damage and the electrical potentials are complicated and generally not available. But estimated electrical potentials could be obtained if a number of finite element calculations are carried out from electrical potentials determined by discrete combinations of damage location and size. Thus, a sample without surface damage and sixteen models with damage location and size evenly distributed in the domain are first processed to retain the reference data. The electrodes A and B are endowed with 10V and 0V as the boundary condition during the course.

After the forward procedure, an estimated relation between surface damage and reference electrical potentials will be obtained. Thus, when a set of input measurement values are given, the surface damage generates these measurement values is supposed to be attained by analyzing these “visible information”. However, it should be noticed that,

it is possible to get several sets of location and size values by the same measurement values. It is understandable since two different combinations of location and size may cause similar measurement values, the seven electrical potential values here V_1-V_7, respectively. Also, when the size of the surface damage is very small, the estimation will be less accurate. That is because small damage size influences the electrical potential distribution less.

2.2 Relationship between damage and electrical potential change

Existence of surface damage can influence the electrical behavior of the laminate. From electrodes mounted on the top surface of the sample, reference measurements of electrical potentials can be directly obtained. For different surface damage situation, the measurement values differ a lot. There exists a relation between these values and the location and size variables. However, due to the complexity of the laminated structure, it is impossible to get this nature relation. Though precise nature relation between potential values and surface damage parameters are difficult and even impossible to be obtained, a forward solution is still necessary for upcoming inverse procedure. Here, finite element calculations are carried out to establish such damage-potential relation for various damage situations. In an iterative type of inverse analysis, the forward solutions are referenced during updating. But if calculations are performed for every estimate, the total number of calculations will be very large and it will be very time-consuming. Thus, a forward solution that relates the surface damage parameters to measured parameters is established prior to the error minimization process. As mentioned before, a domain where location and size values are restricted in is already set. Then sixteen sets of location and size values evenly distributed in the whole domain are picked out to be performed firstly. These damage parameters are chosen to generate the reference electrical potentials. To approximate the potential values at other combinations of s and d, the bi-cubic Lagrangian interpolation function is utilized. With this approach, the total number of required computations is kept at a reasonable level.

The electrical potential value at αth electrode, $V_\alpha(s, d)$, is expressed as a continuous function of damage parameters as:

$$V_\alpha(s,d) \approx \sum_{i=1}^{p}\sum_{j=1}^{q} V_\alpha(s_i,d_j)N_{ij}(s,d) \tag{1}$$

$$N_{ij}(s,d) = \prod_{m=1,m\neq i}^{p} \frac{s-s_m}{s_i-s_m} \prod_{n=1,n\neq j}^{q} \frac{d-d_n}{d_j-d_n} \tag{2}$$

Here, s_i is ith sample point within the range of damage location, d_j is jth sample point within the range of damage size, and N_{ij} is the bi-cubic Lagrangian interpolation function. In this model, seven reference points are picked, so α should range from 1 to 7. Also, altogether sixteen damages are selected to generate the reference data, thus p and q should be endowed with 4. As mentioned before, in this study, the range of location values is $50 < s/t < 200$, while for size values, it is $4 < d/t < 40$. By this equation, the reference potential values with any damage parameters could be calculated.

To show how potential values distribute in the s-d domain under equation (1), the potential at 3rd electrode located at $x/t = 100$ is expressed as a function of damage location and size in figure 3. Here, the potential is normalized by the reference potential V^{ref}, which corresponds to the potential without damage.

From figure 3, smooth surface of potential values is observed. Since only sixteen damages are considered to get the reference measurements, the detailed circumstance could not be accurately displayed. But on the contrary, if more reference models are simulated to obtain more reference data, it will certainly increase the work load. It is accept or reject between efficiency and accuracy. Thus, if good estimation could already be achieved under current reference data, there is no need to use more reference models.

2.3 Error objective function

To extract the unknown parameters, s and d here, the inverse analysis method requires the difference between the actual measurements of electrical potentials and the ones corresponding to estimated damage parameters to be minimized. If s^{est} and d^{est} are the estimated damage location and size, respectively, then the error object function for n electrical potential measurements can be formulated as:

$$\varphi(s,d) = \frac{1}{n}\sum_{i=1}^{n}\left(\frac{V_i(s^{est},d^{est}) - V_i^{meas}}{V_i^{meas} - V_i^{ref}}\right)^2 \tag{3}$$

Here, as shown in the model in figure 1, the number of potential measurement is selected as n = 7. The index "i" denotes one of the seven reference points, V_i^{meas} denoted the corresponding actual measurements of potentials and V_i^{ref} denotes the corresponding potential value in the no damage situation. The electrical potentials for estimated damage parameters are calculated using equation (1) and (2).

By minimizing the error object function, the best estimation of damage parameters should be obtained. And this searching for best estimates procedure is performed by the downhill simplex method, which is discussed next.

2.4 Downhill simplex method

Downhill simplex method is one of the most popular multi-dimensional optimization methods when derivatives of objective function are either unavailable or discontinuous. It was first mentioned by Nelder and Mead in 1965 and it is also called Nelder-Mead method or amoeba method. Downhill simplex method is a numerical method for minimizing an error object function in a many-dimensional space.

The method uses the concept of a simplex, which is a polytope of N+1verticals in N dimensions. In the present work, with two unknown parameters here, the shape of simplex is a triangle for the optimization process and a simplex is defined through three points or sets of estimates. The first point can be chosen arbitrarily within the domain. The other two points are chosen in such a manner that they enclose a non-degenerate area. Since some estimates might get trapped in valleys (i.e., local minima), it is necessary to choose many different sets of initial estimates. In the present analysis, the number of initial points chosen is 304(=16×19) within the domain. The three vertices forming the initial simplex are adjacent to each other and form a right-angled triangle.

For the three points in any initial simplex, each point corresponds to an object error calculated by the error object function. The point with the largest error is considered to be the worst point and it will be replaced by some certain movement and then a new simplex is formed. After a series of moves of the points, the simplex will at last locate in a region and the points shrink to the estimation point which is considered to be a local minimum. The estimated point with the smallest object error among the local minima is

then confirmed as the best estimation. Details of the downhill simplex method are described in Appendix A.

3. Application to 2D damage model

3.1 Identification with electrical potential measurements

Initially, only electrical potential measurements V_1-V_7 were used to determine the unknown parameters. To verify the proposed approach, a prescribed surface damage was applied with parameters s/t = 75 and d/t = 30. With this specified surface damage, after the finite element calculation, simulated electrical potential measurements were provided to the inverse procedure. The corresponding normalized potentials V_1-V_7 in this case are shown in figure 4a. As shown in the figure, the electrical potentials change almost at the same rate for electrodes located on the right of the damage. This is because the electrical current flows from left to right along the sample, and the electrical current value is smaller compared to the no damage situation. Thus, the change rate of these potentials is the same as the change rate of the electrical current since the potentials have a linear relationship with the current. However, at the region where the damage is located, the relationship between the potential and the current is more complicated and the change rate is no longer the same. From the results, it is predicted that using the seven potentials as the measurement variables, the estimation of the damage location must be very accurate.

With these results as input, the error object function in (3) was minimized with the downhill simplex method. The results are shown in figure 4b. There are 304 initial points chosen and the downhill simplex method was performed for each case. For every initial point, it will generate an initial simplex and after some movements, the simplex will at last shrinks to a point. Theoretically, all the 304 initial points will converge into the estimated point which should be close to the exact solution. However, sometimes it is possible to have more than one "valley" during the inverse analysis procedure and thus maybe the 304 initial points will at last converge into more than one point. In this situation, the estimated point whose object error is the smallest will be selected as the "global minimum" and that point will be considered as the final estimated solution. In figure 4b, the estimated points show very fine convergence and they almost converge into the same point. The estimated damage location and size are s/t = 75.8 and d/t = 31.8.

Compared to the exact solution, the estimated damage parameters are very close to the real situation and this result is acceptable.

Since in this experiment, only electrical potentials detected on seven voltage electrodes are used as the reference data, the method used to obtain these data is EPCM. Moreover, ERCM has also been proved to be very effective and here in order to further improve the accuracy of the estimation, a new variable was added as a measurement value. Due to the constant voltage difference between the two current electrodes *A* and *B*, the resistance between these two has an inversely proportional relation with the electrical current in the sample. Thus, the electrical resistance value between *A* and *B* is adopted as the new added measurement and the value could be calculated by transverse electrical current value in the sample. The details are described in the next section.

3.2 Identification by adding electrical resistance measurement

Though the estimated results are already very fine by taking the electrical potentials as the inputs, with the aim to see the impact of combining ERCM with EPCM, the electrical resistance was added to the original inputs. Note that electrical current is an equivalent expression of the resistance between electrodes *A* and *B* since the electrical potential difference between these two is constant. As predicted, damage size will influence the resistance value significantly so the damage size estimation is possible refined well.

With the additional input, the error object function is then modified as:

$$\varphi(s,d)=\frac{1}{n}\sum_{i=1}^{n}\left(\frac{V_i(s^{est},d^{est})-V_i^{meas}}{V_i^{meas}-V_i^{ref}}\right)^2+\left(\frac{R(s^{est},d^{est})-R^{meas}}{R^{meas}-R^{ref}}\right)^2 \tag{4}$$

Here, R^{ref} is the reference electrical resistance when the laminate contains no surface damage. And the forward solution, $R(s^{est}, d^{est})$, is constructed in a similar manner as the resistances from finite element calculations. The electrical resistances between *A* and *B* for various combinations of damage location and size are shown in figure 5.

As predicted above, the electrical resistance values are observed to change quickly with the damage size. Moreover, when the size is small, the electrical resistance

value is almost uniform along the location coordinate. Thus, adding the resistance value is regarded as an effective way to improve the damage size estimation.

To exam the accuracy, surface damage parameters with $s/t = 75$ and $d/t = 30$ were again tested. For this model, the resistance along the sample was computed as $R^{meas}/R^{ref} = 1.05$. This additional information is supplied in the object function (4), and φ is minimized in the downhill simplex method. The local and global minima obtained are shown in figure 6.

The best estimates corresponding to the global minimum were identified as $s/t = 77.2$ and $d/t = 30.4$. Compared to measurements without resistance situation, certainly, the accuracy of the damage size estimation has been improved. However, the estimation of the damage location is not as accuracy as before. Meanwhile, estimates with both object functions are acceptable since they are both close enough to the exact solution. In industry, damage size may be considered more important compared to the location since it will influence the material stiffness directly. In this way, when high level of damage size estimation is required, ERCM maybe a better choice.

The convergence behavior is also influenced by particular values of damage sizes and locations. For completeness, the inverse analysis was performed for different sets of damage parameters. To further verify the procedure using object equation (4), another model with damage parameters $s/t = 140$ and $d/t = 12$ was applied. Estimated global and local minima are shown in figure 7.

Perfect convergence for the local minima is also observed here and the estimated global minimum is close enough to the exact damage parameters, thus the estimation is acceptable. The estimated location and size values are $s/t = 135.3$ and $d/t = 11.7$.

Noted that actual experiment measurements always contain some errors, so in order for this method to be robust, it must be able to determine accurate estimates under various conditions. The estimation behavior when measurements contain errors is studied in the next section.

3.3 Error sensitivity analysis

Estimates of an inverse analysis are influenced by errors contained in the measurements. To check how the estimation accuracy is affected when errors are introduced is an important part to ensure the assessment integrity. In real experiments, errors can be carried out due to contact between electrodes and composites laminates. Also, instrumental errors always exist when detecting the electrical potential or resistance values. Although averaged potentials and resistance can be simply applied as the reference solutions, if deviations arising from the averaging are small, this effect can be included as one factor in the error sensitivity analysis. The deviations are considered to be limited as instrumental errors are considered the error source. If contact problem is occurred, estimations could be far from the real situation. Thus, good contact must be assured when electrodes are mounted on the laminates.

In the detailed error sensitivity analysis, simulated measurements were perturbed with additional small values randomly. Though not shown here, by applying the boundary conditions mentioned above, in the given damage location and size domain, the maximum difference between reference potentials with and without damage is about 0.4V for all seven electrodes. The maximum bound of errors are set to be 5% of this value for potential measurements, which is 0.02V, respectively. The measurement values V_i^{meas} in error object function (4) is then substituted with

$$V_i^{\mathrm{mod}} = V_i^{meas} + r \times 0.4 \times 0.05 \tag{5}$$

As for the same reason, since the maximum difference between reference resistance with and without damage is 0.08Ω in the domain, the electrical current value is modified as:

$$R^{\mathrm{mod}} = R^{meas} + r \times 0.08 \times 0.05 \tag{6}$$

Here, r is a random number between -1 and 1.

As predicted, by adding additional derivations to the measurement values, the estimated location and size values will get away from the exact values compared to the results when no errors are introduced. Since 5% is considered to be a reasonable range for errors, if estimates are still close enough to the exact solution, then this inverse analysis method is taken as “resistant” to errors. If not, the method will be considered error sensitive.

Random errors were added to these measurements and the downhill simplex method was performed for 50 different cases for case $s/t = 75$ and $d/t = 30$. The resulting global minima are shown in figure 8. The global minima are clustered in a small domain very close to the exact solution. This shows that highly accurate estimates are obtained even with the measurement errors. The same procedure was also performed for $s/h = 140$ and $d/t = 12$ case. The resulting global minima are shown in figure 9.

4. Extension to 3D damage model

In this initial study to test the proposed method, it was applied to 2D models. Based on the successful verification of the proposed damage identification method in 2D situation, the inverse analysis approach is then applied for 3D composite laminates. In 3D situation, surface damage is still represented by damage location and size. However, since the location is defined by two parameters here, a surface damage is represented with three variables now. Taking downhill simplex method as the inverse analysis approach again, the number of reference damage models with damages evenly distributed in the location-size domain extends to 64. Also, due to the extra unknown parameter, the accuracy of estimation is doubtful. The specific details of imposed damage and model are described next.

4.1 Surface damage model

To verify the inverse analysis procedure, a eight-ply $[0/90/0/90]_s$ composite laminate is constructed as shown in figure 10. The model is shaped as a hexahedron containing laminates with different fiber orientations and the cross section of the model is square. In the coordinate system shown in the figure, the fiber directions along the x coordinate are defined to be 0^o. Meanwhile, the fiber directions of the layers perpendicular to that is defined as 90^o, which is along the y coordinate. The electrical conductivities of the materials used in this model are the same as in 2D situation and the values are listed in table 1. In this model, due to interlaced fiber arrangement, the electrical current flux distribution will be more complex than the 2D situation.

The thickness of the model is denoted as t = 1.6mm. The intersection shape for each layer is square and the side length of the model is denoted as l = 100mm. Electrodes made with copper are located at four corners on the top surface. The distance between the two neighboring electrodes is denoted as $a = 0.8l$. Surface damage is located from the bottom layer and it is also in square shape viewing from the top and the side length is denoted as d. As the same in 2D case, the damage depth is set to be constant and the depth is denoted as δ. Here, δ is constantly set to be two layers thickness, which is 0.4mm, respectively. The location of the surface damage is the coordinates of the center of the

surface damage in the proposed coordinate system, which is denoted as x and y. As shown in figure 10, the origins of the x and y coordinate axes are set at the center of the model while origin of z axis is at the bottom of the model.

From the model described, only the information for the surface damage is observed to be unknown. Three parameters are required to describe a specific damage, which are damage location x, y and damage size d, respectively. If the damage depth δ is also considered as an unknown parameter rather than a constant value, the number of reference damage models will then be 256 and the inverse analysis procedure will be more complex. This is described later in section 6.

As the same in 2D situation, when doing the simulation, the FE mesh is created to be uniform in the whole model. Element number is 16 along z-coordinate, which is the thickness direction. Along x and y coordinate directions, the element numbers are both set to be 100. As a result, altogether 160,000 elements are adopted in this model.

Since the element is shaped as hexahedron, as a matter of convenience, the surface damage here is also supposed to be in hexahedron shape located in the bottom two layers. The goal of this inverse analysis approach is to find the location and size information of the surface damage, thus, detailed damage shape influence is not considered.

4.2 Damage identification procedure

In 2D situation, EPCM already is proved effective to search for the best estimates of damage location and size. And also, ERCM is conjectured to be better when to get accurate estimate of damage size. Thus, in 3D situation, ERCM is used as the artifice to estimate the unknown damage parameters. As shown in figure 10, four electrodes are mounted at the corners on the top surface of the laminates. The electrodes are denoted as A, B, C and D. In this way, altogether six resistance values could be utilized as the measurements, which can be later used to inversely estimate the unknown information. The six resistances are AB, AC, AD, BC, BD and CD. To obtain a specific resistance value between two electrodes, one electrode will be set to be 0V first and the other one will be charged with 1A electrical current, then the electrical potential value on that

electrode is equal to the resistance value between the electrode pair. This can be easily achieved both ways in experiment and computer simulation.

Most part of the inverse analysis procedure is just the same as in the 2D situation. However, making use of downhill simplex method, the reference damage models now are more complex. In 2D situation, only two variables are supposed to be estimated. But now, the variable number becomes three. Thus, the simplex is a tetrahedron instead of a triangle. When creating the reference damages, now 64 reference models are used to get the reference measurements. A domain of damage location and size is also set here during the process. The x and y coordinates of reference damages are both range from -30mm to 30mm and the size of damage d ranges from 0mm to 12mm.

The locations of the reference surface damages are distributed at sixteen positions. At each position, four damage sizes are considered. Equations (1) and (2) are the expression of bi-cubic Lagrangian interpolation method and this method can also be used in 3D case to calculate the resistance values at any point in the proposed damage variables domain. The algorithm expression in 3D case is modified as:

$$R_\alpha(x, y, \mathrm{d}) \approx \sum_{i=1}^{p}\sum_{j=1}^{q}\sum_{k=1}^{r} R_\alpha(x_i, y_j, d_k) N_{ijk}(x, y, d) \tag{7}$$

$$N_{ijk}(x, y, d) = \prod_{m=1, m\neq i}^{p} \frac{x - x_m}{x_i - x_m} \prod_{n=1, n\neq j}^{q} \frac{y - y_n}{y_j - y_n} \prod_{l=1, l\neq k}^{r} \frac{d - d_n}{d_j - d_n} \tag{8}$$

Here, α ranges from 1 to 6 and the values of p, q, r are endowed with 4. $N_{ijk}(x, y, d)$ is the shape function.

With this interpolation function, by providing the measurement resistance values of reference damage models, the resistance values for any specific damage could be obtained. Thus, the forward procedure is achieved.

For the backward procedure, since there is not too much difference from the 2D situation, the details are not repeated again. The error object function used in the 3D case is shown in equation (9).

$$\varphi(x, y, d) = \frac{1}{n}\sum_{\alpha=1}^{n}\left(\frac{R_\alpha(x^{est}, y^{est}, d^{est}) - R_\alpha{}^{meas}}{R_\alpha{}^{ref}}\right)^2 \tag{9}$$

Here, n equals 6 since six resistances are used as measurements. Meanwhile, R_α^{meas} and R_α^{ref} express for the input resistances obtained from unknown damage model and no damage model.

4.3 Verification study

Downhill simplex method has already been proved efficient to get accurate estimates of damage location and size in 2D situation. However, in 3D case, three unknowns need to be estimated and surely it proposes a bigger challenge for the estimation accuracy. As to verify the inverse analysis procedure, a set of prescribed surface damages distributed at various positions are applied. The comparison of the exact and estimated damage parameters are listed in table 2.

From the results shown in table 2, good match for estimates is observed for damages located near the diagonal or side of square *ABCD* shown in figure 11. It is acceptable because when damage is located near the diagonals or sides, at least one of the measurement resistances will be greatly influenced compared to other damage locations. However, if damage location is not in this way, the estimated results are observed not good enough. For the damage to be x = 21mm, y = -5mm and d = 10mm listed in table 2, the estimation error for damage size is 11.3% and this error is not as accurate as in 2D situation. In order to increase the estimation accuracy of the unknown parameters, two methods may be helpful. One method is to decrease the model size l and the other is to change the positions where voltage electrodes are located. That is because by changing electrodes locations, different resistance measurements are adopted. Thus, the locations of the electrodes are an important fact to influence the estimated results. The details of how to arrange the electrodes and set the electrode spacing are described in the next section.

5. Comparison of electrode arrangements

In the previous section, inverse analysis procedure in 3D situation is verified for a specific model and electrode arrangement pattern. However, in a real large CFRP sample containing damages inside, usually a lot of electrodes need to be mounted to divide the composite into small regions first. Then in a specific region, detecting the surface damage could be accomplishable. In computer simulation, only the smallest cell is used for calculation and it is called the basic model. Hundreds of ways could be applied to arrange the electrodes besides the way mentioned above and how to choose the right one to mount the electrodes is an important subject. Besides, the electrodes spacing between two adjacent electrodes is also crucial. Of course it is easy to figure out that, with more electrodes to collect information, the estimation accuracy could be better. Generally speaking, the aim for an arrangement is to use fewer electrodes to get good estimation accuracy of damage parameters.

5.1 Various arrangements

In order to determine optimum electrode network to detect surface damage, various models are established and their damage detection performances are evaluated. In actual application, it is important to determine the smallest size of damage that can be diagnosed by the network of electrodes. Thus for a given spacing or density of electrodes, various analyses were carried out to determine the robustness of the damage detection. Second, the pattern of electrodes influences the accuracy of damage estimate. Here two most common arrangements, Square and Hexagonal arrays of electrodes as shown in figures 11 and 12 are considered.

The laminate is modeled as a 8-layer cross-ply with $[0/90/0/90]_s$ arrangement. Since the direction of cross-ply orientation may affect the sensitivities of damage detection, two models are also considered for the Square Pattern. One is Square 0^o pattern with the directions of electrodes parallel to either 0^o or 90^o fiber directions, and the other is Square 45^o pattern with the fiber direction along the diagonal direction of electrodes.

Thus, altogether, three patterns, Square 0^o, Square 45^o and Hexagonal, are proposed for comparison using the inverse analysis method. In computer calculation, for

each pattern, the basic models are used instead of taking the whole sample with large amount of electrodes. The electrodes mounted on basic models for different patterns are illustrated in figures 11 and 12. As noticed here, the model mentioned in section 4 is the Square 0^o pattern.

Downhill simplex method requires chosen resistance measurements as the input information. Depending upon the number of electrodes in a chosen cell, there are various combinations of resistances between electrode pairs. For example, in a four electrode square cell, there are six electrode pairs as shown in figure 11. In the hexagonal array with seven electrodes in a cell, twenty-one pairs are possible. When to choosing resistances as measurement inputs, part or all of these pairs could be adopted. When doing computational calculation for Hexagonal pattern, the prescribed damage location as shown in figure 12 and as a result, eight resistances were adopted as the measurements as shown in the figure. That is because these eight resistances influence the measurements more than others.

In this initial verification study, a damaged section is assumed to exist within each cell, and the resistance changes due to the damage are computed. Prior to estimating the damage parameters, a reference data set must be established by carrying out many 3D finite element calculations. Then from a given set of resistance changes and using the Downhill Simplex method, the best estimates for damage are obtained.

5.2 Damage size estimates

Although the post-processing procedure estimates the in-plane location of the damage, in reality, more critical information is the size of damage. For one reason, the damage size is closely related to the composite stiffness. On the other hand, the estimation accuracy trend of damage location is similar to damage size in most time. In the simulations, the damage shape is set be a square with the side length d as shown in figure 10. Initially, the damage depth δ is assumed to be a quarter of laminate thickness or equivalent to two plies thickness ($\delta/t = 0.25$). The anisotropic electrical conductivities of laminate are chosen as σ_0 = 5,500 S/m, σ_{90} = 204 S/m and σ_T = 20.7 S/m as listed in table 1.

As described before, the aim for an arrangement is to use fewer electrodes to get good estimation accuracy of damage parameters. Thus, a new variable ρ is brought out to measure the electrode numbers in unit area and ρ is called electrode density. When the estimation accuracy values for the three patterns are the same, the pattern with the smallest electrode density is considered to be the best since fewer electrodes are used for that pattern to obtain that estimation accuracy. The distance between two nearby electrodes is defined to be a, which is shown in figure 10 for all three patterns. Then for Square pattern, the electrode density can be expressed as $\rho = 1/a^2$ and for Hexagonal pattern, as $\rho \cong 1.16/a^2$.

In the basic model for a specific pattern, there are altogether five parameters, electrode density ρ (or a), model thickness t and the three damage parameters, x, y and d, respectively. For the damage size estimate, the estimation accuracy is related to electrode density of course, and it is also influenced by the surface damage size d. Meanwhile, the model thickness t is also possible to have an effect on the accuracy. Comparison of the three patterns for each variable is described next.

5.2.1 Effects of electrode density

In this initial analysis, the estimates are obtained for various spacing between electrodes while the damage size is kept $d \cong 10$mm. For each electrode arrangement pattern, inverse procedure is performed for five different values of a while the other parameters are the same. The model thickness is set to be 1.6mm as before and since the damage depth is a quarter of t, it is also constantly equal to 0.4mm. Needless to say, to avoid the effect of input damage location, all the to-be-detect damages are set to be relatively in the same position, that is, x/a and y/a are set to be constant.

The estimation accuracy of size varies from different electrode density. It is predicable that the estimation error will be incremental while the electrode density decreases for each pattern. The comparisons of estimated and input damage information for the three patterns are shown in tables 3-5. As shown in the tables, the damages are set to be located at $x = 0.2625a$, $y = -0.0625a$. When model size is small, for each pattern, the damage size estimation will be accurate. Moreover, the relations between electrode

density and damage size estimation are then illustrated in a figure. Since electrode density is defined to be inversely proportional to a^2, the parameter ρd^2 will be dimensionless. Damage size is set to be around 10mm, so then the variation of the size estimation error with ρd^2 will show the relation between estimation accuracy and electrode density. The variation for each pattern is shown in figure 13.

Figure 13 shows that for each pattern, size estimation error decreases while electrode density gets bigger. Also, when ρ approaches to zero, the error will increase more quickly. From this figure, it should be noticed that, the damage size estimation does not differ too much for the three patterns. But generally speaking, among these three patterns, with the chosen resistances as reference measurements, Square 0^o is observed to be the best. That is because for the same estimation error requirement, to detect the same size damage, the electrode density of Square 0^o is the smallest. Also, between Square 0^o and Square 45^o patterns, the estimation difference is even smaller. Then the influence of cross-ply orientation is considered to be small.

If 10% is considered to be an acceptable size estimation error, then Square 0^o pattern needs ρd^2 to be more than 0.18. In other words, electrodes spacing a should be no smaller than 80mm.

5.2.2 Effects of damage size

Estimation accuracy is certainly related to the damage size. A bigger damage will become easier to be precisely detected since the measurement resistances change bigger. Taking Square 0^o for example, with ρ to be constant instead, the size estimation error should decrease when d gets bigger. In table 6, estimation errors are listed for five different damage size when a = 80mm. Taking the dimensionless parameter ρd^2 as the reference again, the change of estimation error is shown in figure 14 in broken red line. Figure 14 also shows the comparison with the same model while changing electrode density. Since a domain is prescribed for the damage size, when a is set to be 80mm, the biggest value of ρd^2 that can be obtained is 0.0225. But for the curve by changing electrode density, ρd^2 could range from 0 to 0.07. However, in the same part in the

domain of ρd^2, it is observed that these two curves almost obey the same trend and for the same value of ρd^2, the estimation error difference is small.

Also, from the results shown in table 6, it is observed that when damage size is around 10mm, the estimation error for this case is around 10%. And for smaller damage sizes, estimation could not be considered to be good enough. To increase this estimation accuracy, more electrode pairs could be utilized besides the previous six measurements. This is discussed in section 6.3.

5.2.3 Effects of model thickness

Previously, damage size estimates are proved to be related to electrode density and input damage size itself. However, there is another model parameter to be examined. Whether the model thickness t is related to the estimated results or not is unclear since this can not be concluded by common sense. To check this, the Square 0^o pattern model with electrode spacing a = 80mm, damage location x = 21mm, y = -5mm and damage size d = 10mm is tested by different model thickness values. The results are shown in table 7 and illustrated in figure 15. During the procedure, the damage depth was always set to be a quarter of the whole model thickness, that is, δ/t is constant.

From the results, it is observed that the size estimation error does not change with the model thickness and the estimation error is always around 14%. From the regression curve, it is observed that when the ratio of damage depth to model thickness is constant, the size estimation will hardly change with variation of model thickness.

5.3 Relationship between estimation error and resistance change

To estimate a prescribed surface damage, using the downhill simplex method, reference damage models should be calculated and this is time-consuming. However, if estimation error could be obtained only by the resistance changes due to the prescribed damage, things could be much easier, because in this way, there is no need to calculate the reference models any more.

For a specific arrangement with fixed model size, there exists a linear relation between estimation error of size and resistance changes from prescribed damage. Taking

the Square 0^o pattern for example, with model size a = 80mm and model thickness t = 1.6mm, many prescribed damages were estimated. For a specific damage, the six resistance measurements will change from the resistances without damage and the norm of resistance changes is shown in as:

$$\left\| \frac{\Delta R}{R} \right\|_{norm} = \sqrt{\sum_{i=1}^{n} \left(\frac{\Delta R_i}{R_i} \right)^2} \tag{10}$$

The relation between estimation error and norm of resistance changes is shown in figure 16. From the figure, it is observed that it is a roughly linear relationship between them. Thus, if not exact estimated results should be obtained, to get a rough estimation error of damage size, only the resistance change information of that damage is necessary.

6. Estimated damage size and depth

In the inverse analysis approach in 3D situation, previously, the damage depth is set to be constant and yet only three variables are to be estimated. However, in real situation, the damage depth also can be unknown. Adding damage depth δ as the forth unknown parameter, when using the downhill simplex method as the inverse analysis method, the reference damage models extend to 256. The computer calculation load is heavy and also the estimation accuracy is called in doubt.

6.1 Model description

Taking the Square 0^o pattern as the basic model and setting the model parameters all the same as before as described in section 4, the inverse analysis approach was performed again. The electrode spacing used here is a = 80mm and model thickness is set to be t = 1.6mm. Damage location both range from -30mm to 30mm and damage size ranges from 0 to 12mm. Since in most time, the damage thickness will not exceed half of the model thickness, the maximum damage depth is set to be 0.375t. It should be noticed that the reason for arising the domain for each parameter is for the convenience to build the reference models. Of course, after setting the domain for all the unknown parameters, only damage in this domain could be estimated.

When there is no damage exists in the laminate, the six resistances could be easily obtained and the measurements are used for reference values. If a specific input damage is located in the laminate, the resistance values will be influenced and the effect is based on the damage information. To see how the resistance changes vary with different damage size and depth, specific damage models with damage location to be x = 21mm and y = -5mm are calculated again. After damage location is set, the resistances for any damage size and depth could be obtained by the forward procedure. The normalized resistance AD for discrete damage size and depth in the d-δ domain are shown in figure 17. It is observed when damage is very small, the resistance changes little and in this way, it will be harder to get accurate estimates. Resistance information is also shown in figure 18 with the change of the damage size in 2D plot. From figure 18, it is observed that resistance change increases when damage size or depth increases. For a specific depth, it

is not a linear relation between normalized resistance and damage size. With damage size gets bigger, the resistance increases much more quickly.

With the inverse analysis approach described before, estimated results with the same damage location are listed in table 8. Estimation accuracy of damage is expressed with damage size and depth. The error for estimated damage parameters is expressed as:

$$error = \sqrt{\frac{(\frac{d^{est} - d^{exa}}{d^{exa}})^2 + (\frac{\delta^{est} - \delta^{exa}}{\delta^{exa}})^2}{2}} \tag{11}$$

Here, d^{est} and d^{exa} refer to estimated damage size and exact damage size. It is the same for damage depth.

With the calculation results by equation (11), the relation between estimation errors and damage size and depth is shown in figure 19. The regression curves are obtained by given five input damages. From the analysis above, damages with depth 0.5mm should have better estimates compare to depth to be 0.4mm situation. However, it is observed that the estimation for damage depth to be 0.4mm is the best and this is against the fact that larger damage will result in better estimation accuracy. This is because for $\delta =$ 0.4mm, the damage occupies two entire layers, but for $\delta =$ 0.5mm, the damage occupies two and a half layers. Since the fiber directions of two contiguous layers are different, it will be easier to estimate damage with depth to be multiple of one layer thickness.

6.2. Error sensitivity analysis in 3D situation

In 2D situation, error sensitivity analysis was made by adding extra error to measurements. In 3D situation, the detailed error sensitivity analysis is performed again. Instead of adding random errors, 5% errors of the maximum difference between damage and no damage models for every resistance were added to the measurements. Then the modified measurement resistances are then replaced in equation 9. Since similar procedure was already done in 2D situation, the details would not be described again.

Many calculations were done for specific input damages. Measurements with errors were used to get the estimates and also the estimated results with no errors in

measurements are listed for comparison in table 9. As predicted, by adding additional derivations to the measurement values, the estimated values will get far away from the exact values compared to the results when no errors are introduced. For damage to be x = 21mm, y = -5mm, d = 8mm and δ = 0.4mm, the estimation error for damage raises from 12.3% to 42.5%. It surely makes the estimation too bad to be acceptable by adding measurements. For the other damages listed in the table, all the estimation errors increase largely. The size estimation errors for these four input damages are shown in figure 20. Figure 20 clearly show the large error increment after adding measurement noise.

In 2D situation, estimation is considered to be "resistant" to errors. However, in 3D situation, due to extra damage parameters compared to 2D situation, the estimation is sensitive to noise.

6.3. Accuracy improvement by adding extra measurements

In section 6.1, damage estimation with six measurement resistances were performed. However, in a large plane with many electrodes mounted on the surface, various resistances could be adopted as the measurements besides the previous described ones. It is understandable that with more resistances as the measurements, the damage estimation accuracy could be improved. This is because more information is available now in the whole procedure.

To prove that, with the same parameters in section 6.1 for example, more resistance values are calculated. Extra resistances between electrode pairs are shown in figure 21 with the expression of broken lines and the measurements become 11 resistances. By providing five more measurements, now the estimation accuracy becomes more precise and results for some input damages are listed in table 10. For damage to be x = 21mm, y = -5mm, d = 8mm and δ = 0.4mm, the estimation error for damage decreases from 12.3% to 3.5%. This can be considered to be a great improvement for estimation. For other cases, damage estimation all observed to be largely improved. Thus, adding more measurements could be regarded as an effective way to improve damage estimation.

Measurement noise was also added in this situation and the estimated results are shown in table 10 for comparison. Figure 20 also illustrates the size estimation error increment due to measurement noise in this situation.

7. Measurements from actual CFRP laminates

Damage detection of CFRP laminates is proved to be successful by computer simulation. However, experiments for real CFRP sample should be made for the integrity of the analysis. Though damage detection for the whole inverse procedure was not shown by experiments on CFRP samples, additional tests were carried out on CFRP with Direct Write electrode.

7.1 Specimen and measurements

Additional tests were carried out on CFRP with direct write electrode deposited as shown in figure 22. First, to measure the effect of straining on their electrical resistance, the unidirectional fiber laminate (Graphtek, LLC) was placed in a tensile machine (TIRA test 260005). No load resistance between two middle electrodes was measured as $R_o \cong$ 1.012Ω. The sample was loaded to ~80N or about the axial stress of 12MPa. The recorded changes in the resistance are shown in figure 23. Though there are considerable noise and scattering, the general resistence was appeared to be increasing with the load. The reference strain was also measured by a commercial gage attached on the laminate as shwon in figure 24. Based on the axial strain of up to about 100 microstrain and the regression cuver, the gage factor of CFRP is approximated as 20.4. However further study is needed to confirm this value. The approximated Young's modulus of the composite was 138GPa, which is within the range of common unidirectional carbon fiber reinforced composites.

In order to measure the resistance change due to damage, the back surface of specimen was grit blasted with alumina particles as shown in figure 24. Essentially this removed carbon fibers and epoxy matrix. An apporximated damage areas is 8mm wide and remaining thickness was about 0.3mm, representing about 40% thickness removal. The resistance between the electrodes was measured again as $R_{damage} \cong$ 1.338Ω or $R / R_o \cong$ 32.2%.

7.2 Finite element simulations

To investigate the effect of damage further, a finite element model was set up to simulate the resistance change by the damage. Since the volume fraction of fibers and actual electrical conductivity of CFRP are the sample are not known, the following data by Todoroki et al [6] shown in table 11. Here σ_0, σ_{90} and σ_T are the electrical cunductivies along the fiber direction, the in-plane perpendicular or 90^o direction and the through-thickness direction, respectively. Several FE calculations are performed to match with the measured resistivity between the two copper electrodes. The resistivity of copper is set as 58.8×10^6 S/m. Note that the through-thickness conudctivty is very low since the laminate generally contains epoxy-rich regions at their interlayers. Afer several computations, we determined the best fit to be $\sigma_0 \cong$ 5,200S/m, $\sigma_{90} \cong$ 140S/m and $\sigma_T \cong$ 14S/m for the CFRP laminate. This corresponds to the fiber volume fraction to be $V_f \cong$ 56% which is likely to be close to the actual value.

The simulations are also carried out with these estimated properties for the laminate with damage as shown in figure 24. The computed resistences against electrical flow near the damage are shown in figure 25. Here the parameter essentially represents the product of resistance and electrical flow. Large resistances are seen immediately near the electrodes and also near the damaged surface. Due to the electrical flow through thinner section, the resistance between the electrodes increases. The resistances between two electrodes are computed for various extents of damage depths. Here the damage depth or the remaining thickness of laminate is assumed to be uniform for the damage region (width 8mm) and the resulting resistances are obtained as shown in figure 26. Here the resistance increases with the damage depth. Based on the measured resistance ($R_{damage} \cong 1.34\Omega$), the estimated damage is $\delta/t = 0.48$ or remaining thickness of ~0.27mm. This value is close to the approximately measured remaininig thickness at the damage (shown in figure 24).

8. Discussion

A novel approach based on an inverse analysis technique was proposed to identify surface damages in composite panels. The scheme was developed as an alternative approach to more costly flaw detection techniques. Electrical potentials and resistances were chosen as possible measurements. Applicability of a stochastic procedure, the downhill simplex method, was demonstrated as a potential tool in the identification of unknown damage parameters. In the verification analysis, both 2D and 3D situations were considered. In 2D situation, a four-ply laminate was used as the test model and simulated measurements were obtained for different values of damage size and location. In 3D situation, an eight-ply laminate was used as the test model and similar way was applied. With the chosen electrical resistance or potential measurements, the proposed procedure yields to accurate estimates.

To clearly illustrate the steps of the inverse analysis procedure, the flowchart of 2D situation is outlined in figure 27. First, in order to construct forward/reference solutions a priori, measurable parameters are constructed as approximate and continuous functions of unknown damage parameters using finite element calculations and interpolation functions. This approach reduces the computational cost during the search process. Secondly, the error objective function that expresses the accuracy of estimates is clearly established. Thirdly, the downhill simplex method is utilized to search values corresponding to the minimal objective function. The technique is very effective when gradients of objective function are not available. At last, the error sensitivity study confirms the robustness of the proposed method even with expected measurement errors.

In 3D situation in the other hand, the procedure is just the same except using different measurements and different error objective function. Also, there are more unknown parameters which require more reference models. However, except for that, more work was done in 3D situation. When arranging electrodes on the sample, different ways were proposed and they may result in different estimation accuracy. Three different patterns were tested and compared to see the effect of arrangement patterns and fiber orientations. The relation between estimation accuracy and model size and thickness were

also tested by a lot of calculations. At last, inverse analysis procedure was performed again for the situation when damage depth was also unknown.

There are some limitations for this whole inverse method. First, the proposed method does not assume other types of damage in the composite (e.g., delaminations between layers). If they are present, electrical resistance and potential measurements will be affected and the damage information will not be precisely estimated. Second, when comparing the three patterns, different measurements used for estimation could result in different estimated results. But for the Hexagonal pattern, only part of the measurements was chosen as measurements, thus it is possible that more accurate results can be obtained if more resistances are chosen as measurements. Third, when comparing the three patterns, due to calculation limitation, only five models were calculated for each pattern. This may not be sufficient to get the detailed relation.

References

[1] F. Aymerich and P. Priolo (2008), Characterization of fracture modes in stitched and unstitched cross-ply laminates subjected to low-velocity impact and compression after impact loading, International Journal of Impact Engineering, 35, p.591–608.
[2] P. Schubel and J. Luo (2007), Impact and post impact behavior of composite sandwich panels, Composites: Part A, 38, p.1051–1057.
[3] Y.I. Oka and K. Okamura (2005), Practical estimation of erosion damage caused by solid particle impact Part 1: Effects of impact parameters on a predictive equation, Wear, 259, p.95–101.
[4] F. Aymerich and S.Meili (2000), Ultrasonic evaluation of matrix damage in impacted composite laminates, Composites: Part B, 31, 1–6.
[5] G. Mook, R. Lange and O. Koeser (2001), Non-destructive characterization of carbon-fibre-reinforced plastics by means of eddy-currents, Composites Science and Technology, 61, p.865–873.
[6] A. Todoroki and M. Tanaka (2002), Measurement of orthotropic electric conductance of CFRP laminates and analysis of the effect on delamination monitoring with an electric resistance change method, Composites Science and Technology, 62, p.619–628.
[7] M. Ueda and A. Todoroki (2008), Delamination monitoring of CFRP laminate using the two-stage electric potential change method with equivalent electric conductivity, Engineering Fracture Mechanics, 75, p.2737–2750.
[8] A. Todoroki, M. Tanaka and Y. Shimamura (2005), Electrical resistance change method for monitoring delaminations of CFRP laminates: effect of spacing between electrodes, Composites Science and Technology, 65, p.37–46.
[9] A. Todoroki, Y. Tanaka and Y. Shimamura (2002), Delamination monitoring of graphite/epoxy laminated composite plate of electric resistance change method, Composites Science and Technology, 62, p.1151-1160.
[10] A. Todoroki, M. Tanaka and Y. Shimamura (2003), High performance estimations of delamination of graphite/epoxy laminates with electric resistance change method, Composites Science and Technology, 63, p.1911-1920.
[11] M. Ueda and A. Todoroki (2006), Asymmetrical dual charge EPCM for delamination monitoring of CFRP laminate, Key Engineering Materials 321-323, p.1309-1315
[12] A. Todoroki (2008), Delamination Monitoring Analysis of CFRP Structures using Multi-Probe Electrical Method, Journal of Intelligent Material Systems and Structures, 19, p. 291 - 298.
[13] Chen PW and Chung DDL (1993), Carbon fibre reinforced concrete for smart structures capable of non-destructive flaw detection, Smart Mater Structure, 2, p.22–30.
[14] X. Wang and Chung DDL (1997), Sensing delamination in a carbon fibre polymer-matrix composite during fatigue by electrical resistance measurement, Polym Compos, 18(6), p.692–700.
[15] K. Schulte and C. Baron (1989), Load and failure analysis of CFRP laminates by means of electrical resistivity measurements, Comp. Sci. Technol, 36, p.63-76.
[16] Frederiksen and P.S. (1997), Experimental procedure and results for the identification of elastic constants of thick orthotropic plates, Journal of Composite Materials, 31, p.360–382.

[17] G. Liu and S. Chen (2001), Flaw detection in sandwich plates based on time-harmonic response using genetic algorithm, Computer Methods in Applied Mechanics and Engineering, 190, p.5505–5514.
[18] S. Ishak., G. Liu, H. Shang and S. Lim (2001), Locating and sizing of delamination in composite laminates using computational and experimental methods, Composites Part B: Engineering, 32, p.287–298.
[19] N. Muto, H. Yanagida, T. Nakatsuji, M. Sugita and Y. Ohtsuka (1993), Preventing Fatal Fractures in Carbon-Fiber–Glass-Fiber-Reinforced Plastic Composites by Monitoring Change in Electrical Resistance, J.AM.Ceram.Soc., 76, p. 875-879
[20] X. Wang and D. D. L. Chung (1997), Sensing delamination in a carbon fiber polymer-matrix composite during fatigue by electrical resistance measurement, Polymer Composite, 18, p. 692-700.
[21] X. Wang and D. D. L. Chung (1998), Self- monitoring of fatigue damage and dynamics strain in carbon fiber polymer-matrix composite, Composite Part B, 18, p. 63-73.
[22] D.D.L. Chung and S. Wang (2003), Self-sensing of damage and strain in carbon fiber polymer-matrix structural composites by electrical resistance measurement, Polym Compos, 11, p. 515–525.
[23] N. Ramanujam, T. Nakamura and M. Urago (2005), Identification of embedded interlaminar flaw using inverse analysis, International Journal of Fracture, 132, p.153–173.
[24] S. Wang, D.P. Kowalik and D.D.L. Chung (2004), Self-sensing attained in carbon fiber polymer-matrix structural composites by using the interlaminar interface as a sensor, Smart Mater Struct 13, p. 570–592.
[25] W.J. Crantwell, P. Curtis and J. Morton (1986), An assessment of the impact performance of CFRP reinforced with high-strain carbon fibres, Compos. Sci. Technol. 25, p. 133–148.
[26] R. Schueler, S.P. Joshi and K. Schulte (2001), Damage detection in CFRP by electrical conductance mapping, Compos. Sci. Technol. 61, p. 921–930.
[27] D.C. Seo and J.J. Lee (1999), Damage detection of CFRP laminates using electrical resistance measurement and neural network, Compos. Struct. 47, p. 525–530.
[28] J.C. Abry, S. Bochard, A. Chateauminois, M. Salvia and G. Giraud (1999), In situ detection of damage in CFRP laminates by electric resistance measurements, Compos. Sci. Technol., 59, p. 925–935.

Appendix A

The downhill simplex method minimizes the objective function by taking a series of steps. This method uses the concept of a simplex, which is a polytope of N+1verticals in N dimensions. Here, downhill simplex method when $N = 2$ is presented as the example to show the detailed procedure, corresponding to 2D situation. The shape of the simplex chosen here is a triangle defined by a set of three points.

Suppose p_1, p_2 and p_3 are denoted as three points on s-d plane and the objective functions at these points are set to be $\varphi(p_1) < \varphi(p_2) < \varphi(p_3)$, where $p_1 = (s_1, d_1)$, $p_2 = (s_2, d_2)$ and $p_3 = (s_3, d_3)$, corresponding to three different surface damage parameters. The four types of steps are outlined below. Note that the aim of the moves is to move the simplex closer to the exact solution of the problem.

Step 1: Reflection - This step moves the highest point with the value of objective function to be the largest among the three through the opposite face of the simplex to a supposedly lower point (where the value of the objective function is expected to be lower than at the highest point). Thereby the triangle flips by 180^o. The reflected point p_r is found as

$$p_r = 2p_m - p_3 \tag{A.1}$$

Here, $p_m = (p_1 + p_2)/2$. Note that the highest point here is p_3. Most of the steps in downhill simplex method are reflections.

Step 2: Reflection and expansion - The second type of move is termed as reflection and expansion. This is performed when the value of objective function further drops along the line of reflection of the highest point. This step is designed to further accelerate the process of convergence. The corresponding point p_e is

$$p_e = p_r + (p_m - p_3) \tag{A.2}$$

Step 3: Contraction - This step is usually performed when reflection of the highest point does not cause further decrease in the value of the objective function. The idea here

is that the local minimum lies within the triangle. The point corresponding to contraction p_c is

$$p_c = (p_m - p_3)/2 \tag{A.3}$$

Step 4: Multiple Contraction - This is performed when contraction does not cause a decrease in the objective function of the point under consideration. The lowest point here is p_1. So, there are two new points to be evaluated here. Let them be denoted as p^2_{mc} and p^3_{mc}. They are found as

$$p^2_{mc} = (p_1 + p_2)/2 \text{ and } p^3_{mc} = (p_1 + p_3)/2 \quad . \tag{A.4}$$

Here, a total of 304=16×19 points are chosen along the range of damage location *s* and damage size *d*. The various types of steps are geometrically shown in figure 28. The complete flowchart of the downhill simplex method is shown in figure 29. The search process terminates when the step size reaches

$$\left| \frac{\phi^{n+1}(p_1) - \phi^n(p_1)}{\phi^n(p_1)} \right| \le 1 \times 10^{-7} \tag{A.5}$$

or when the number of iterations reaches 1000.

Table 1. Electrical conductivities of copper and carbon fiber reinforced polymer used in simulation. Here, the conductivities for CFRP correspond to the situation when volume fracture of carbon fiber is 60%.

	Copper	Carbon fiber reinforced polymer		
		σ_0	σ_{90}	σ_T
Electrical conductivity (S/m)	5.88×10^7	5500	204	20.7

Table 2. Comparison of input parameters and estimated parameters of surface damage for Square 0^o pattern model with a = 80mm, t = 1.6mm, δ = 0.4mm.

Models		x (mm)	y (mm)	d (mm)	Error of size (%)
1	Input	21.0	-5.0	10.0	11.3
	Estimated	19.34	-7.44	11.13	
2	Input	-15.0	15.0	8.0	-5.9
	Estimated	-13.81	16.32	7.53	
3	Input	25.0	25.0	6.0	-3.8
	Estimated	24.42	26.63	5.77	
4	Input	0.0	0.0	14.0	3.4
	Estimated	0.0	0.0	14.47	

Table 3. Comparison for input and estimated damage parameters by changing electrode density for Square 0^o pattern. The input damages are all located relatively in the same position. Model thickness is set to be t = 1.6mm.

Square 0^o		x (mm)	y (mm)	d (mm)	Error of size (%)
a = 40mm	Input	10.5	-2.5	10	4.3
	Estimated	10.81	-2.78	10.43	
a = 64mm	Input	16.8	-4.0	9.6	8.2
	Estimated	15.23	-2.98	10.39	
a = 80mm	Input	21.0	-5.0	10	11.3
	Estimated	19.34	-7.44	11.13	
a = 96mm	Input	25.2	-6.0	9.6	18.4
	Estimated	21.12	-5.34	11.37	
a = 120mm	Input	31.5	-7.5	10.5	21.7
	Estimated	27.23	-5.49	12.78	

Table 4. Comparison for input and estimated damage parameters by changing electrode density for Square 45^o pattern. The input damages are all located relatively in the same position. Model thickness is set to be t = 1.6mm.

Square 45^o		x (mm)	y (mm)	d (mm)	Error of size (%)
a = 40mm	Input	10.5	-2.5	10	6.3
	Estimated	10.98	-2.75	10.63	
a = 64mm	Input	16.8	-4.0	9.6	11.8
	Estimated	15.79	-2.14	10.73	
a = 80mm	Input	21.0	-5.0	10	13.2
	Estimated	18.23	-7.34	11.32	
a = 96mm	Input	25.2	-6.0	9.6	16.8
	Estimated	23.12	-4.98	11.21	
a = 120mm	Input	31.5	-7.5	10.5	21.4
	Estimated	26.78	-4.98	12.75	

Table 5. Comparison for input and estimated damage parameters by changing electrode density for Hexagonal pattern. The input damages are all located relatively in the same position. Model thickness is set to be t = 1.6mm.

Hexagonal		x (mm)	y (mm)	d (mm)	Error of size (%)
a = 40mm	Input	10.5	-2.5	10	8.3
	Estimated	10.12	-2.64	10.83	
a = 64mm	Input	16.8	-4.0	9.6	13.6
	Estimated	16.56	-3.45	10.91	
a = 80mm	Input	21.0	-5.0	10	18.7
	Estimated	19.78	-6.12	11.87	
a = 96mm	Input	25.2	-6.0	9.6	22.1
	Estimated	23.12	-5.68	11.72	
a = 120mm	Input	31.5	-7.5	10.5	25.4
	Estimated	29.34	-5.76	13.17	

Table 6. Comparison for input and estimated damage parameters by changing input damage size. The input damages are all located in the same position. Model thickness is set to be t = 1.6mm.

Square 0^o		x (mm)	y (mm)	d (mm)	Error of size (%)
a = 80mm	Input	21.0	-5.0	3	22.3
	Estimated	18.12	-8.56	3.67	
	Input	21.0	-5.0	5	19.6
	Estimated	17.26	-7.89	5.98	
	Input	21.0	-5.0	7	17.3
	Estimated	18.14	-7.67	8.21	
	Input	21.0	-5.0	9	14.1
	Estimated	18.34	-6.94	10.27	
	Input	21.0	-5.0	11	8.5
	Estimated	19.84	-6.74	11.93	

Table 7. Comparison for input and estimated damage parameters by changing model thickness. The input damages are all located in the same position. Electrode spacing is set to be a = 80mm.

Square 0°		x (mm)	y (mm)	d (mm)	Error of size (%)
t = 0.8mm	Input	21.0	-5.0	10.0	15.7
	Estimated	19.24	-6.98	11.57	
t = 1.2mm	Input	21.0	-5.0	10.0	14.3
	Estimated	17.90	-6.45	11.43	
t = 1.6mm	Input	21.0	-5.0	10.0	11.3
	Estimated	19.34	-7.44	11.13	
t = 2.0mm	Input	21.0	-5.0	10.0	16.7
	Estimated	22.12	-4.56	11.67	

Table 8. Comparison for input and estimated damage parameters for Square 0^o pattern model with different damage depth. (a = 80mm, t = 1.6mm)

Square 0^o		x (mm)	y (mm)	d (mm)	δ (mm)	Error of damage estimation (%)
a1	Input	21.0	-5.0	4.0	0.3	74.5
	Estimated	20.71	-4.21	2.65	0.59	
a2	Input	21.0	-5.0	6.0	0.3	63.5
	Estimated	17.94	-6.13	3.95	0.54	
a3	Input	21.0	-5.0	8.0	0.3	30.5
	Estimated	29.73	-4.18	11.07	0.24	
a4	Input	21.0	-5.0	10.0	0.3	12.8
	Estimated	25.48	-3.83	11.37	0.26	
a5	Input	21.0	-5.0	12.0	0.3	6.3
	Estimated	23.15	-5.03	12.66	0.27	
b1	Input	21.0	-5.0	4.0	0.4	5.6
	Estimated	20.80	-4.73	3.90	0.42	
b2	Input	21.0	-5.0	6.0	0.4	11.4
	Estimated	22.82	-4.43	6.64	0.34	
b3	Input	21.0	-5.0	8.0	0.4	11.4
	Estimated	24.80	-4.93	8.56	0.34	
b4	Input	21.0	-5.0	10.0	0.4	5.3
	Estimated	22.76	-4.79	10.47	0.37	
b5	Input	21.0	-5.0	12.0	0.4	2.4
	Estimated	21.98	-5.00	12.25	0.38	
c1	Input	21.0	-5.0	4.0	0.5	24.4
	Estimated	19.08	-6.19	4.80	0.35	
c2	Input	21.0	-5.0	6.0	0.5	17.0
	Estimated	27.54	-4.25	5.86	0.61	
c3	Input	21.0	-5.0	8.0	0.5	32.8
	Estimated	21.38	-5.30	10.42	0.32	
c4	Input	21.0	-5.0	10.0	0.5	13.0
	Estimated	23.78	-4.71	9.22	0.58	
c5	Input	21.0	-5.0	12.0	0.5	10.1
	Estimated	21.63	-5.00	11.12	0.56	

Table 9. Estimated results by six measurements with and without measurement noise.

Square 0^o		x (mm)	y (mm)	d (mm)	δ (mm)	Error of damage estimation (%)
1	Input	21.0	-5.0	8.0	0.4	
	No artificial noise	24.80	-4.93	8.56	0.34	12.3
	With artificial noise	25.67	-3.56	9.75	0.18	42.5
2	Input	12.0	18.0	6.0	0.3	
	No artificial noise	13.21	16.89	4.98	0.19	28.2
	With artificial noise	15.34	14.56	3.12	0.16	47.3
3	Input	-15.0	-15.0	10.0	0.5	
	No artificial noise	-14.56	-15.67	9.23	0.46	7.5
	With artificial noise	-13.12	-17.45	8.04	0.37	23.2
4	Input	-25.0	25.0	4.0	0.2	
	No artificial noise	-24.12	25.65	3.14	0.22	17.4
	With artificial noise	-22.15	27.45	3.05	0.27	30.5

Table 10. Estimated results by adding extra five measurements. Measurements with noise are also considered for comparison.

Square 0^o		x (mm)	y (mm)	d (mm)	δ (mm)	Error of damage estimation (%)
1	Input	21.0	-5.0	8.0	0.4	
	Eleven measurements without artificial noise	22.34	-4.92	8.23	0.38	3.5
	Eleven measurements with artificial noise	24.21	-4.12	8.45	0.35	9.4
2	Input	12.0	18.0	6.0	0.3	
	Eleven measurements without artificial noise	12.56	17.23	5.61	0.25	11.4
	Eleven measurements with artificial noise	13.12	16.89	5.32	0.19	26.7
3	Input	-15.0	-15.0	10.0	0.5	
	Eleven measurements without artificial noise	-14.91	-15.12	9.86	0.48	3.0
	Eleven measurements with artificial noise	-14.12	-15.56	9.34	0.40	14.9
4	Input	-25.0	25.0	4.0	0.2	
	Eleven measurements without artificial noise	-24.89	25.23	3.95	0.17	8.5
	Eleven measurements with artificial noise	-24.13	25.78	3.45	0.14	22.1

Table 11. Orthotropic electrical conductivities of different volume fractions of carbon fibers in CFRP.

V_f	σ_0 (S/m)	σ_{90} (S/m)	σ_T (S/m)
0.40	3,700	0.67	0.059
0.47	4,600	5.2	1.01
0.62	5,500	204	20.7

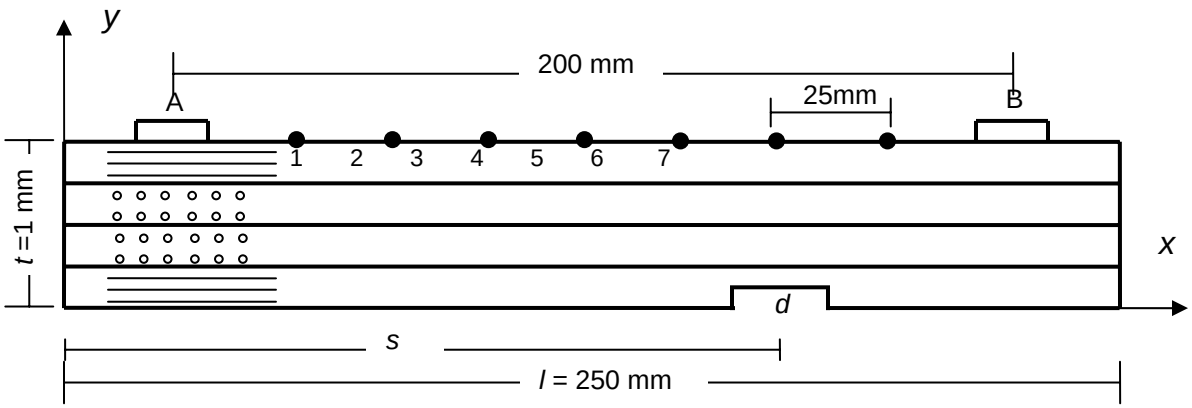

Figure 1. The four-ply $[0/90]_s$ CFRP laminated model used for 2D situation. Two electrodes (4mm×0.25mm) are mounted on the top surface with locations at x = 25mm and x = 225mm. The size of the model is detailed described. Seven voltage electrodes are mounted on the top surface to obtain the measurement potentials. Surface damage is located at the bottom layer with constant damage thickness.

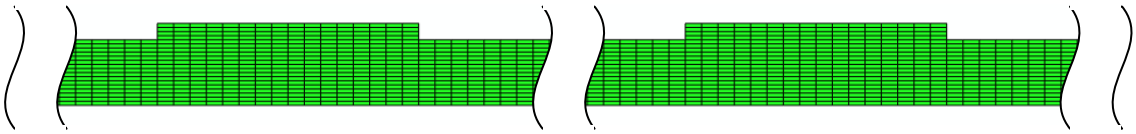

Figure 2. FE mesh of part of the model. The element size is 0.25mm×0.0625mm. The total element number of the model is around 16,000.

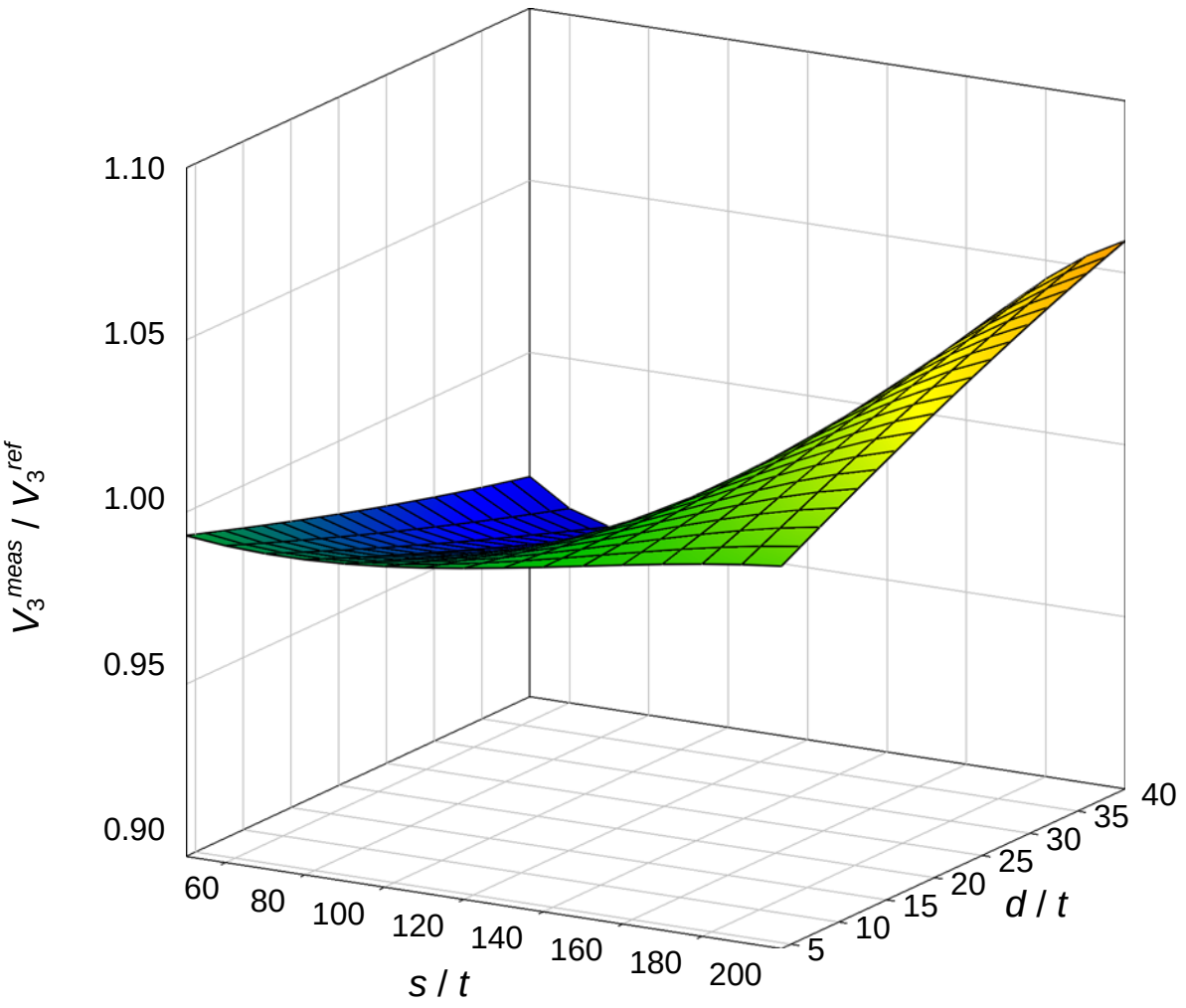

Figure 3. Normalized electrical potential values of 3rd electrode (x = 100mm) for different location and size sets in location-size domain calculated by bi-cubic Lagrangian interpolation function.

(a)

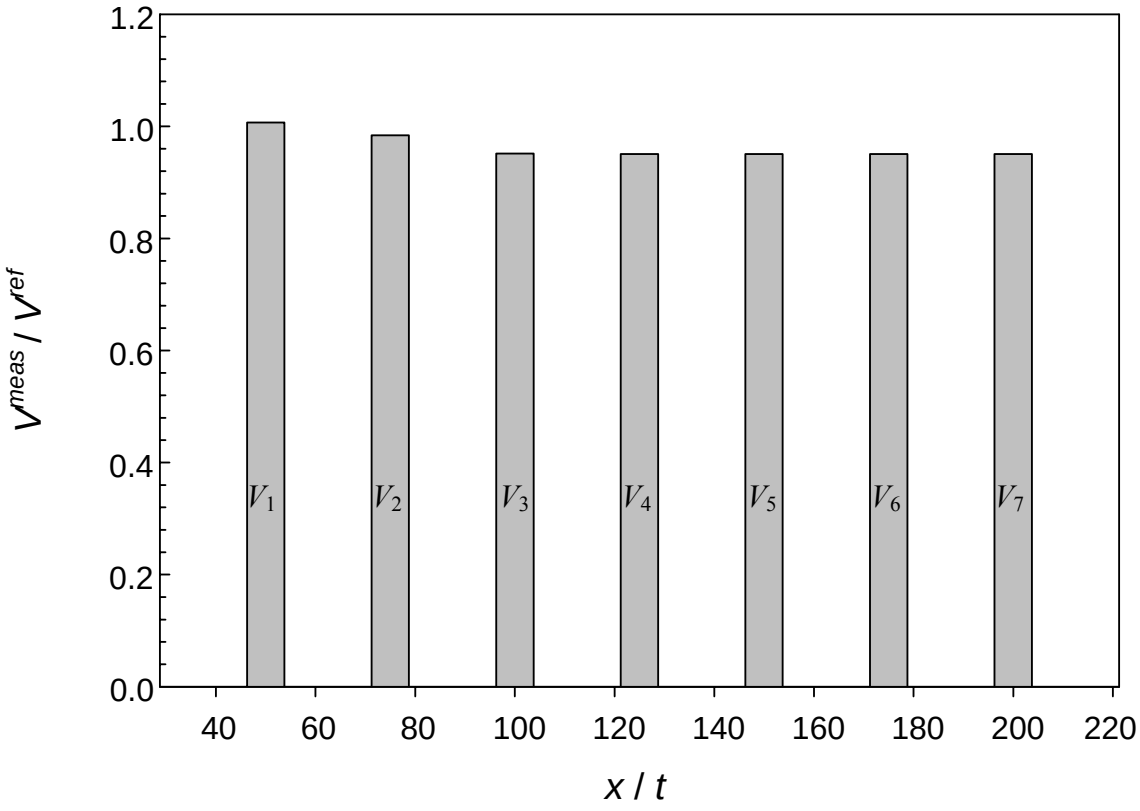
1.2
1.0
0.8
0.6
0.4
0.2
0.0
V^{meas} / V^{ref}
V_1
V_2
V_3
V_4
V_5
V_6
V_7
40
60
80
100
120
140
160
180
200
220
x / t

(b)

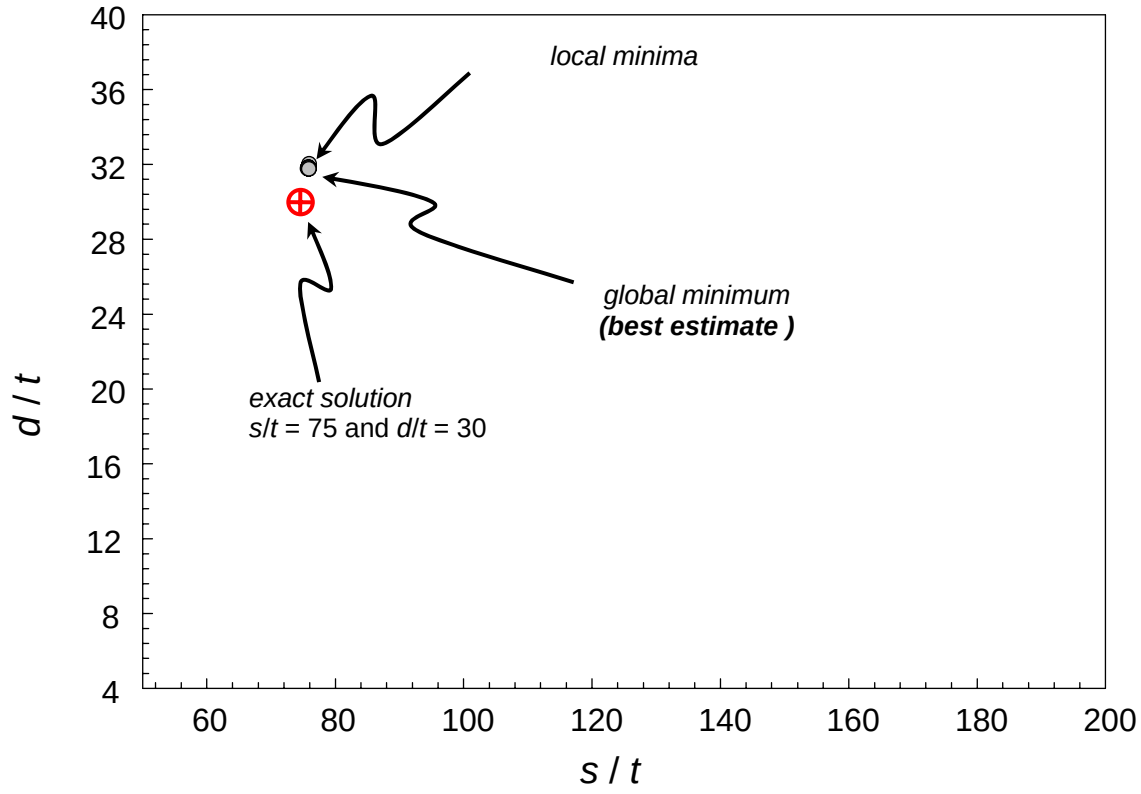

Figure 4. (a) Normalized electrical potentials at seven locations by given boundary conditions for $s/t = 75$ and $d/t = 30$. (b) Local and global minima are shown in the domain of unknown parameters with electrical potential values as the inputs. Exact solution is also shown for reference.

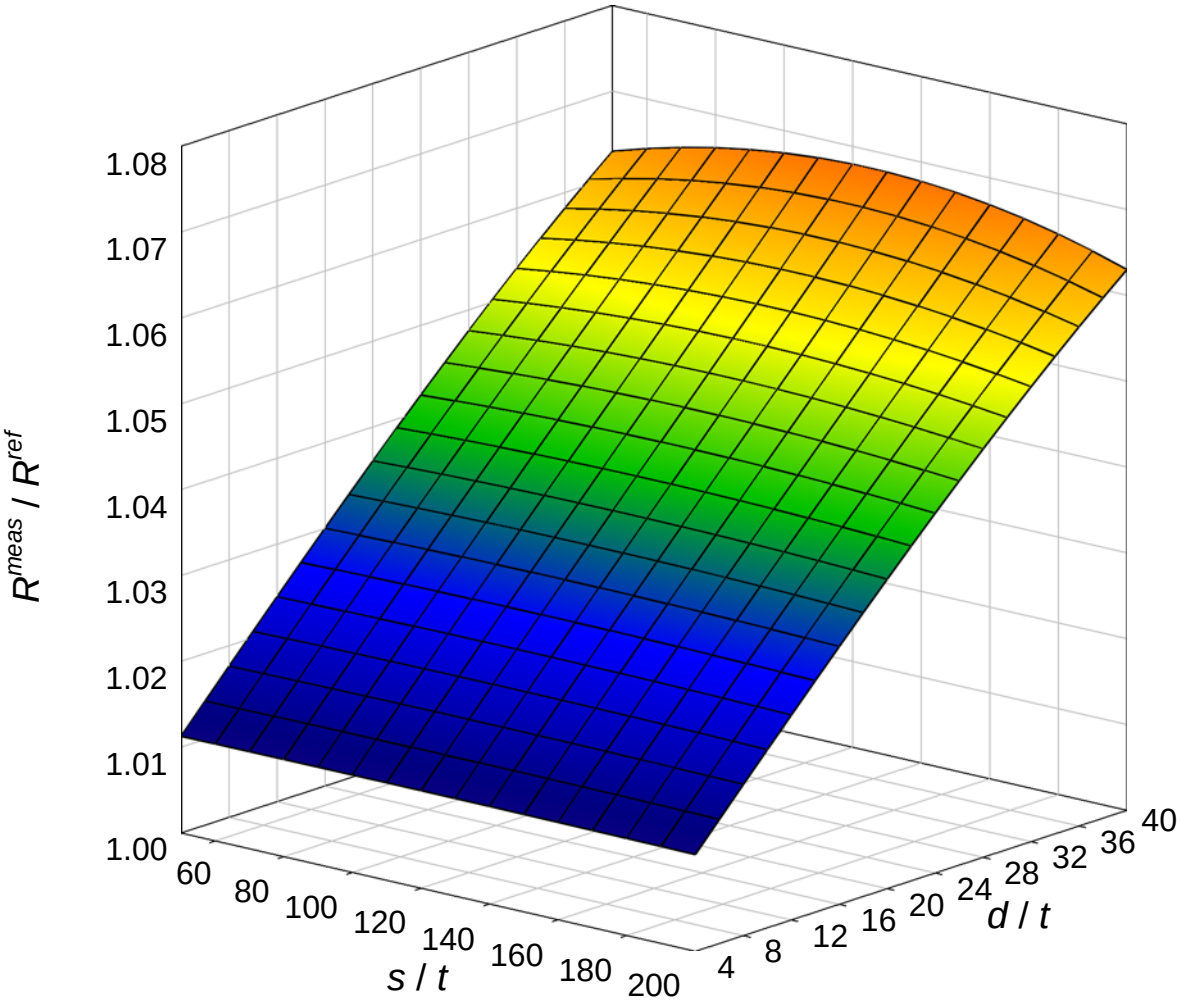

Figure 5. Normalized electrical resistances for various damage locations and sizes. The electrical resistance values are observed to change quickly with the damage size. When damage size is small, the resistances are almost uniform along the location axis.

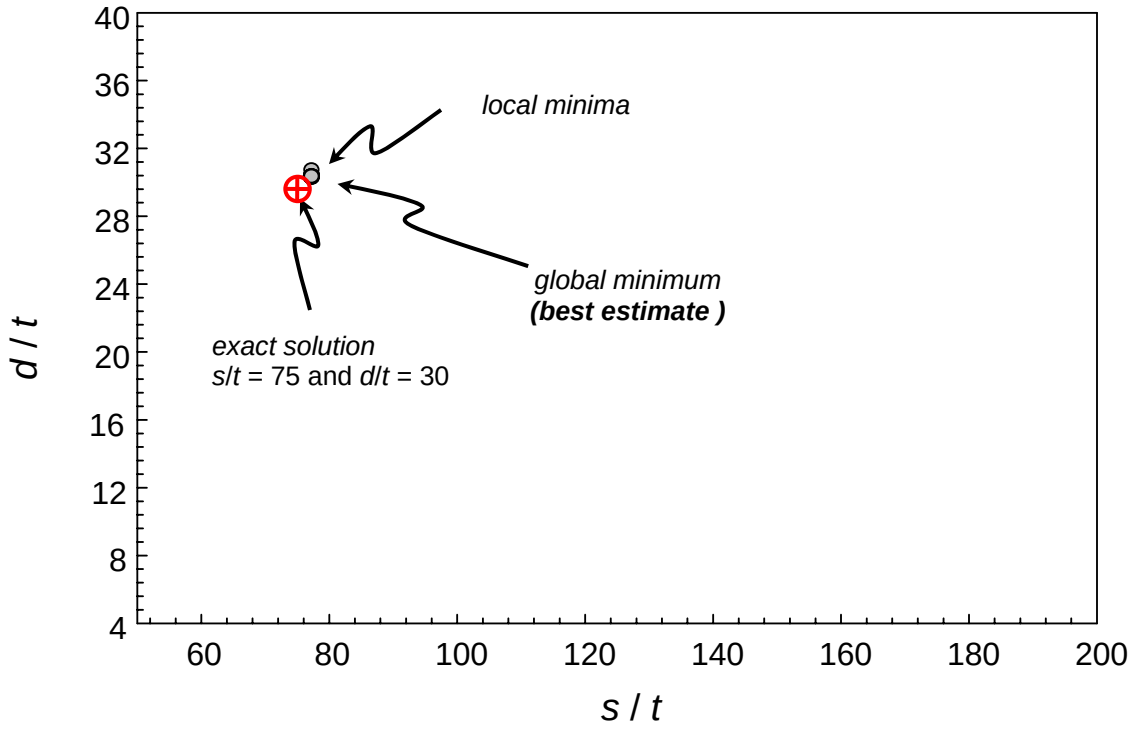

Figure 6. Comparison of estimated results with exact solution $s/t = 75$ and $d/t = 30$ taking electrical potentials and an extra resistance values as inputs. Local minima almost converge into one point shows good convergence of the result. Point with the smallest error object value is chosen to be the best estimate.

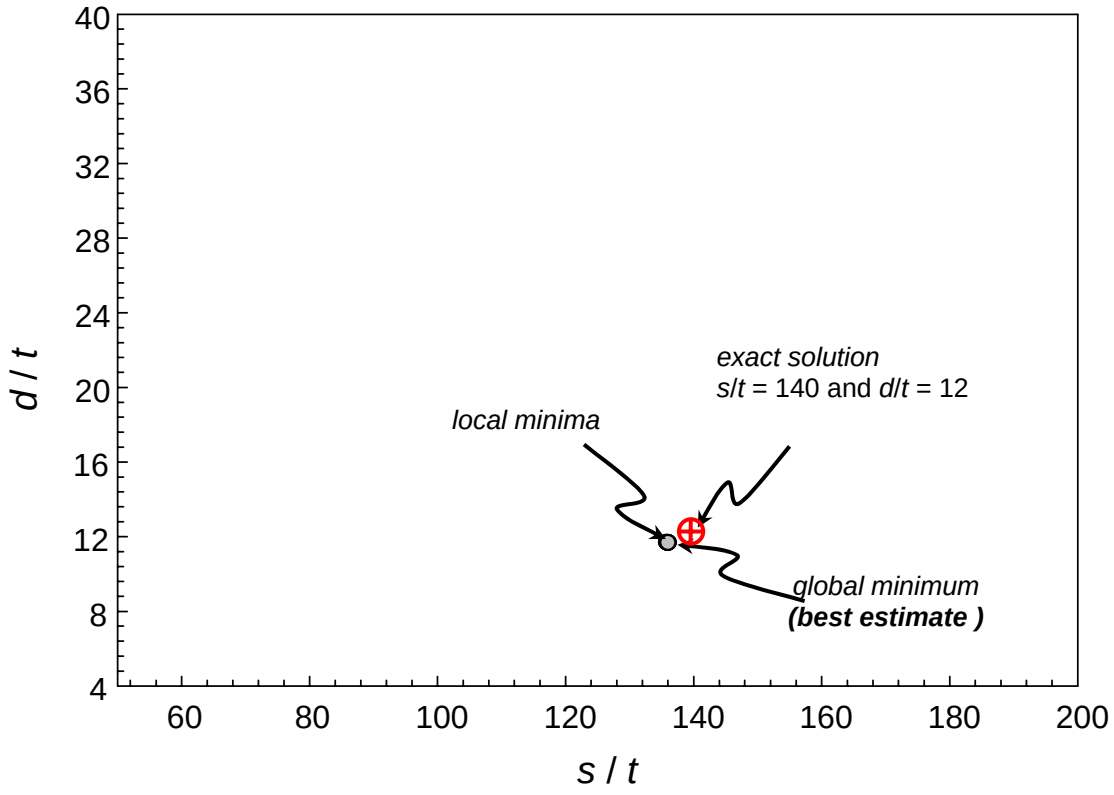

Figure 7. Comparison of estimated results with exact solutions for surface damage s/t = 140 and d/t = 12 taking electrical potentials and an extra resistance values as inputs. Local minima almost converge into one point shows good convergence of the result. Point with the smallest error object value is chosen to be the best estimate.

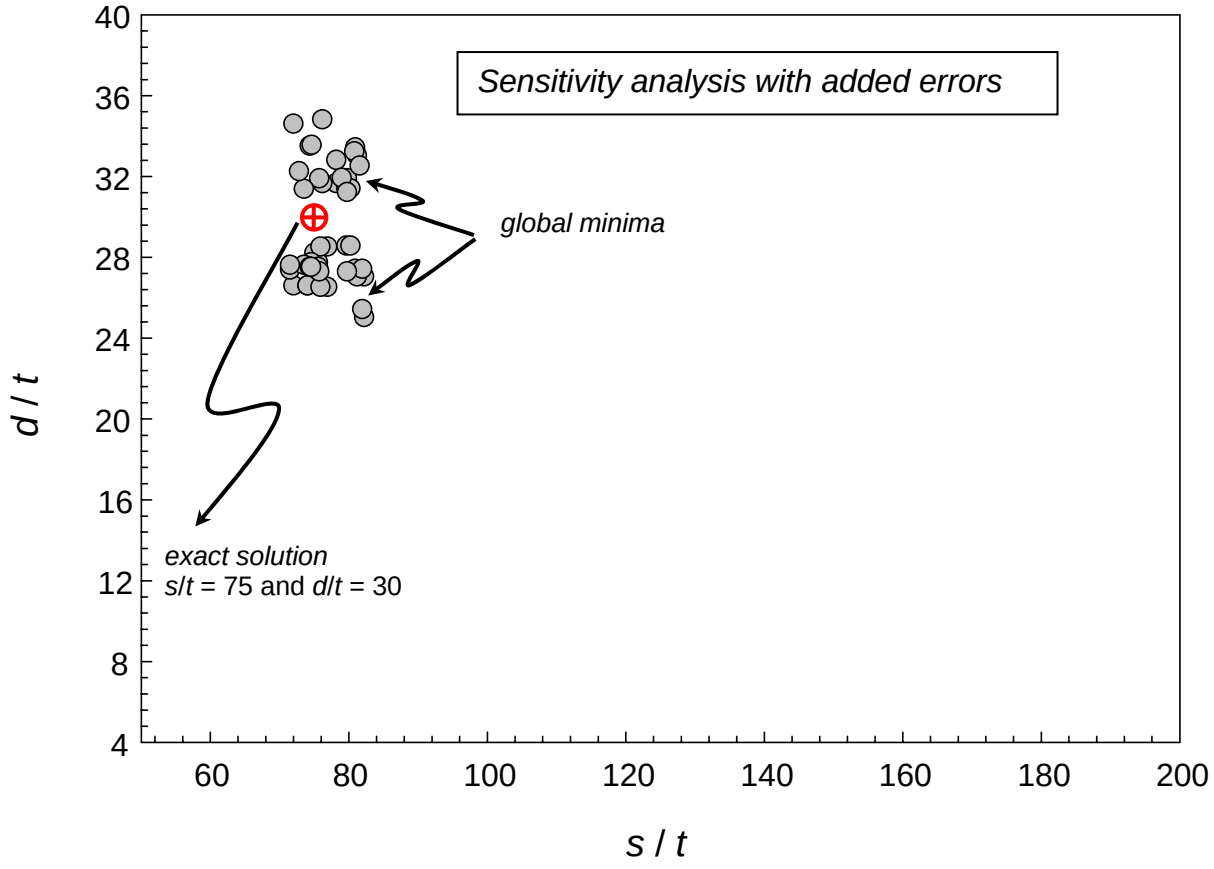

Figure 8. Global minima determined in the error sensitivity analysis are shown for *s/t* = 75 and *d/t*= 30. Here 50 separate analyses (with different random errors added to measurements) are performed in each model. These global minima are identified with seven electrical potentials and one electrical resistance.

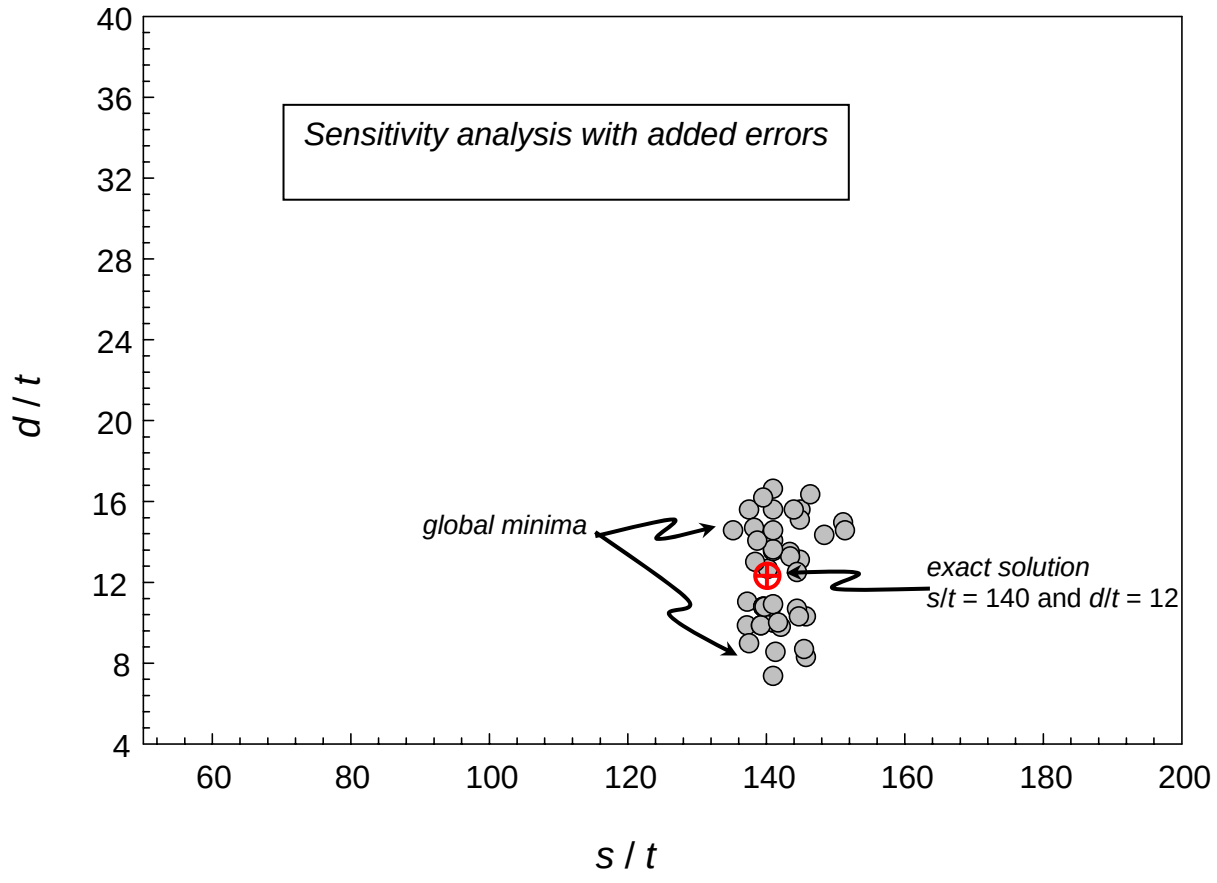

Figure 9. Global minima determined in the error sensitivity analysis are shown for damage $s/t = 140$ and $d/t = 12$. A total of 50 separate analyses (with different random errors added to measurements) are performed in each model. These global minima are identified with seven electrical potentials and one electrical resistance.

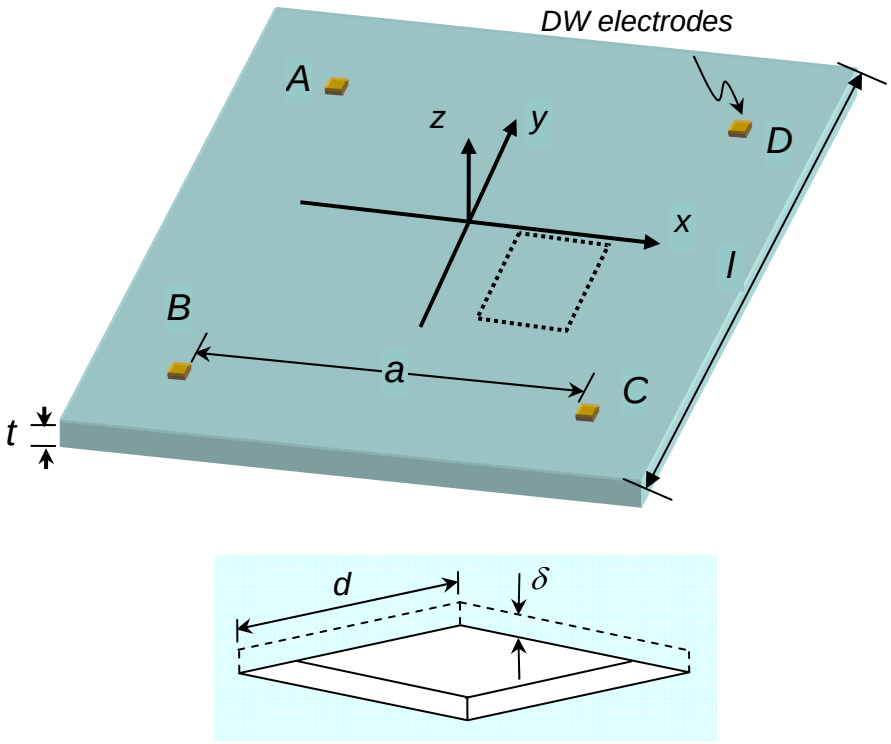

Figure 10. $[0/90/0/90]_s$ composite laminate model used in 3D situation. The side length of the model is *l* and the thickness of the model is *t*. Square shape damage is located from the bottom layer. The size and thickness of the damage are *d* and *δ*. Four electrodes are located at the corners on the top surface.

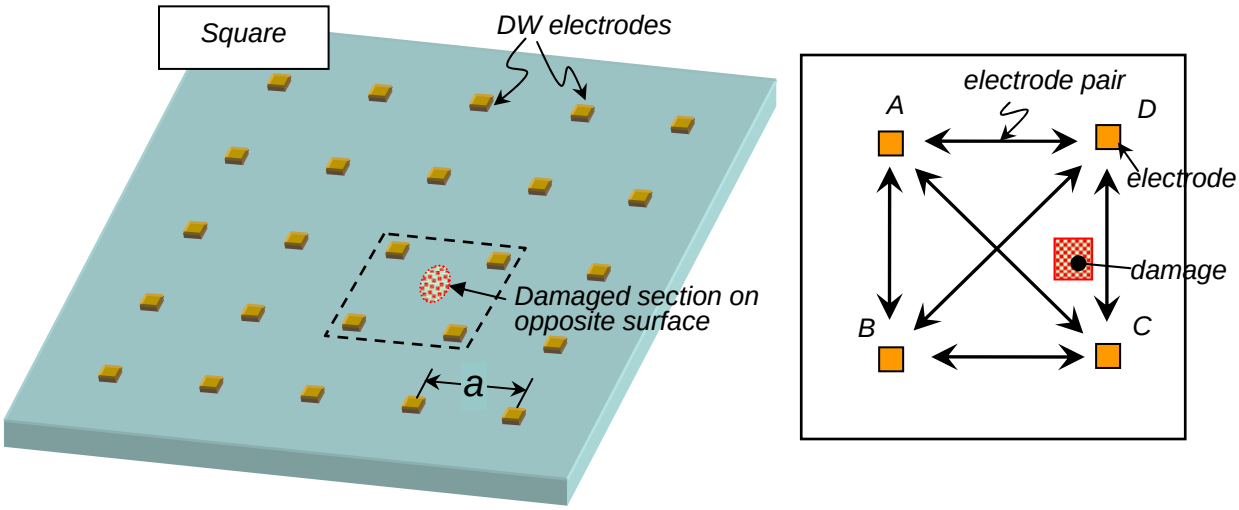

Figure 11. Square pattern takes the smallest cell as square. (a) Considering the effect of cross-ply orientation, for Square pattern, the directions of electrodes parallel to either 0^o or 90^o fiber directions is named as Square 0^o. Fiber direction along the diagonal direction of electrodes is named as Square 45^o. (b) Six resistances are possible to be used in the smallest cell for measurements.

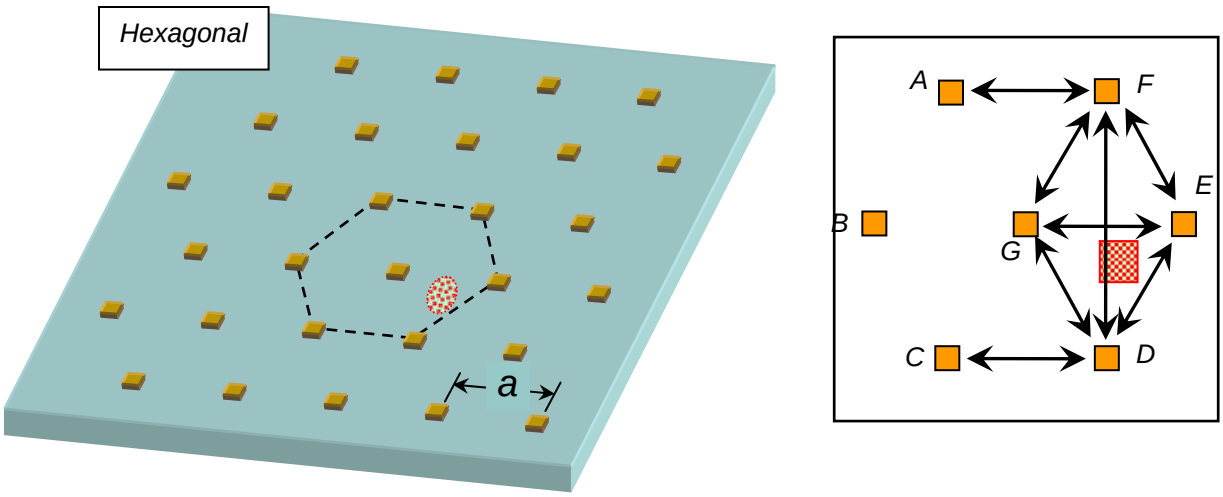

Figure 12. Hexagonal pattern used triangular as the smallest cell. (a) Schematic of possible electrode pairs to measure resistances for hexagonal grids. (b) Twenty-one resistances are possible to be used in the smallest cell for measurements. Eight resistances were used in actual calculation as measurements.

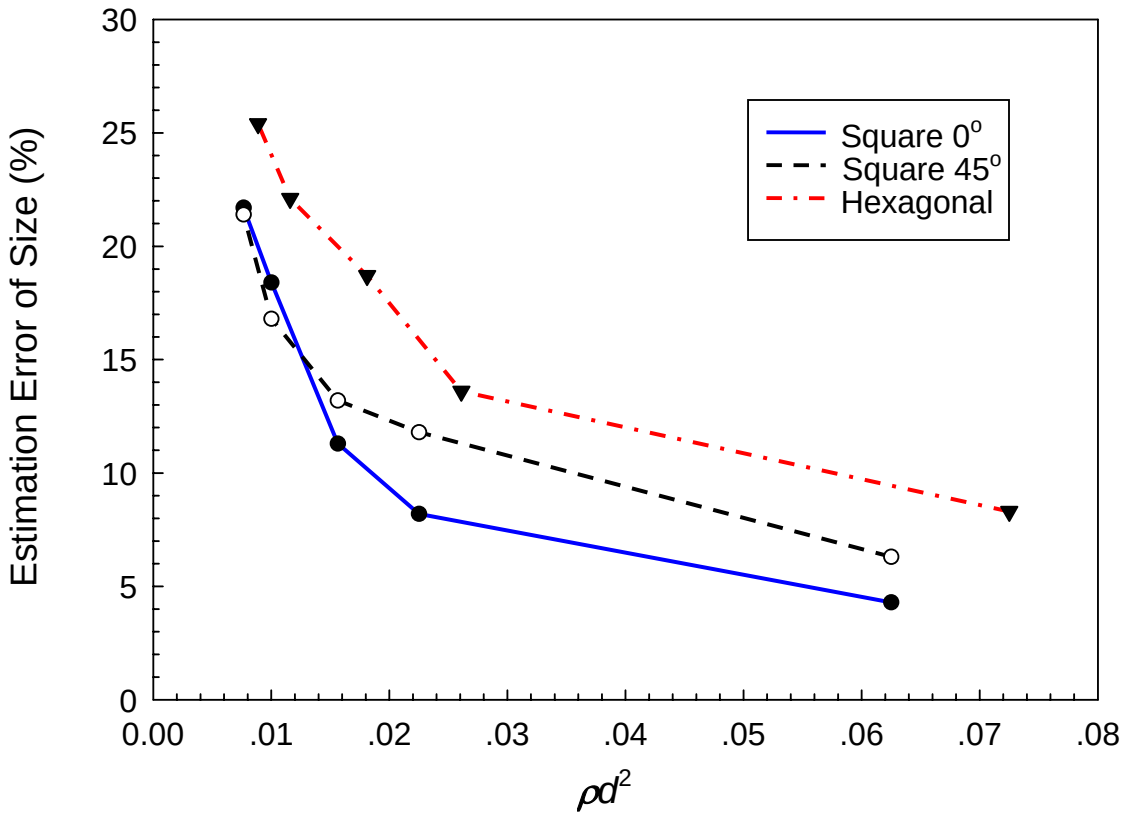

Figure 13. Estimation errors for damage size when changing the electrode density. For each pattern, five damage models are estimated by changing the electrode spacing *a* while keeping other parameters the same.

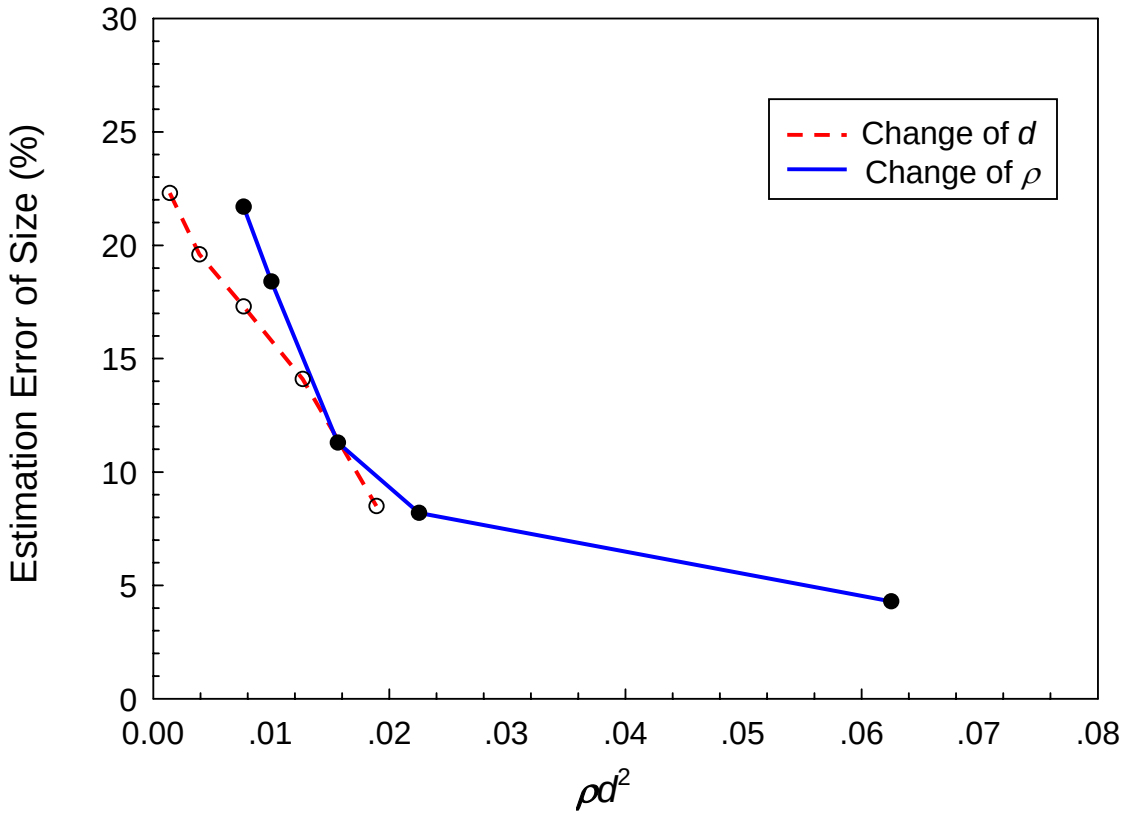

Figure 14. Estimation errors for damage size when changing the size of input damage d. The estimates were calculated for Square 0^o pattern. Estimation errors when changing the electrode density is also illustrated for comparison.

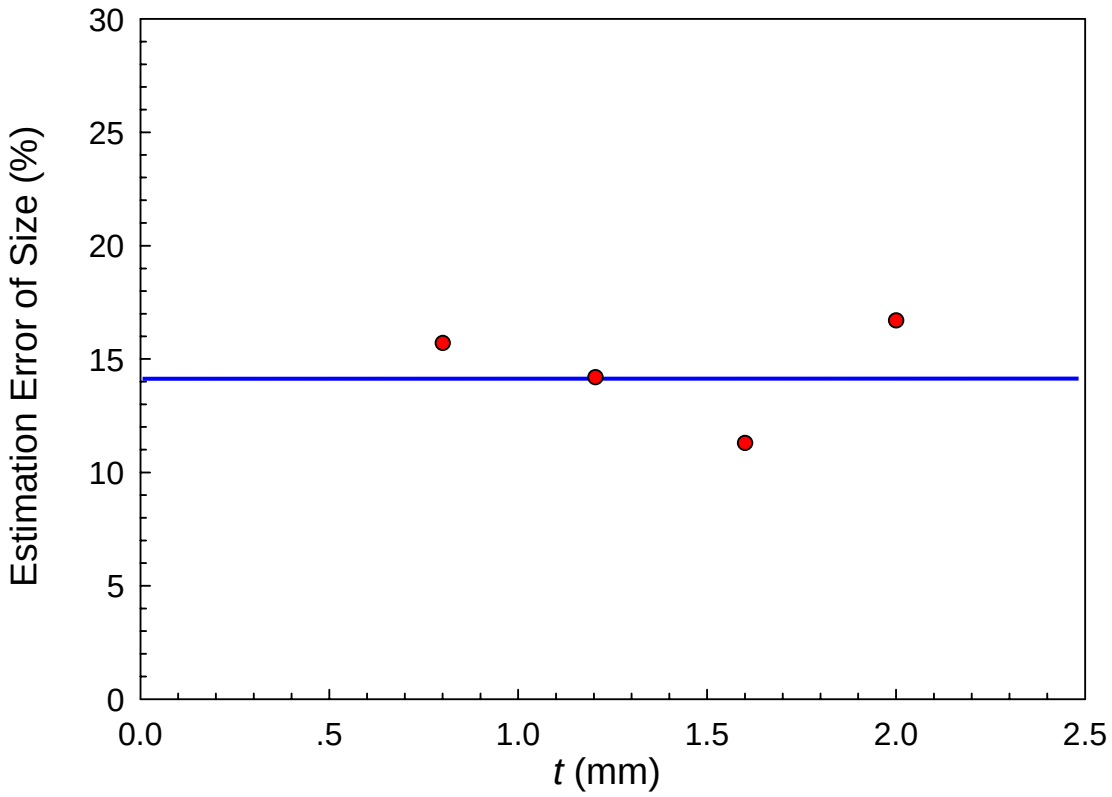

Figure 15. Estimation errors for damage size when changing the model thickness. Regression curve shows that the estimated results are hardly influenced by model thickness t as long as d/t is constant.

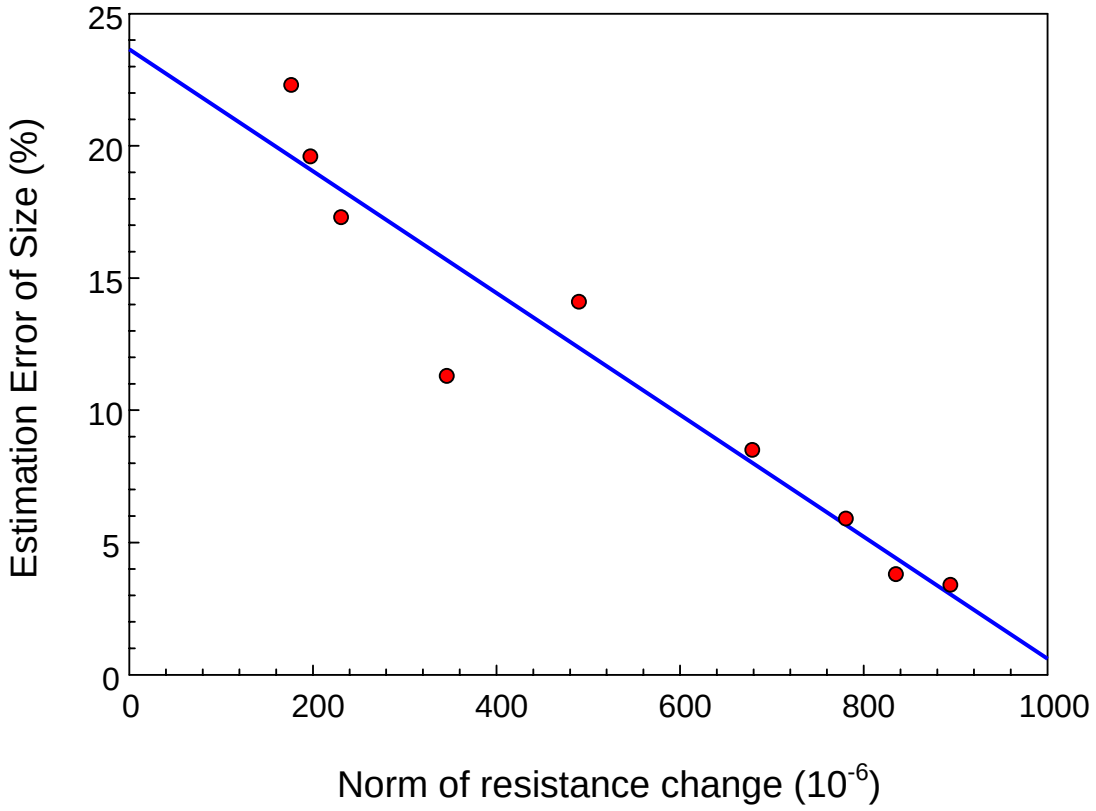

Figure 16. Relationship between size estimation error and norm of resistance change for Square 0^{o} pattern. (a = 80mm, t = 1.6mm)

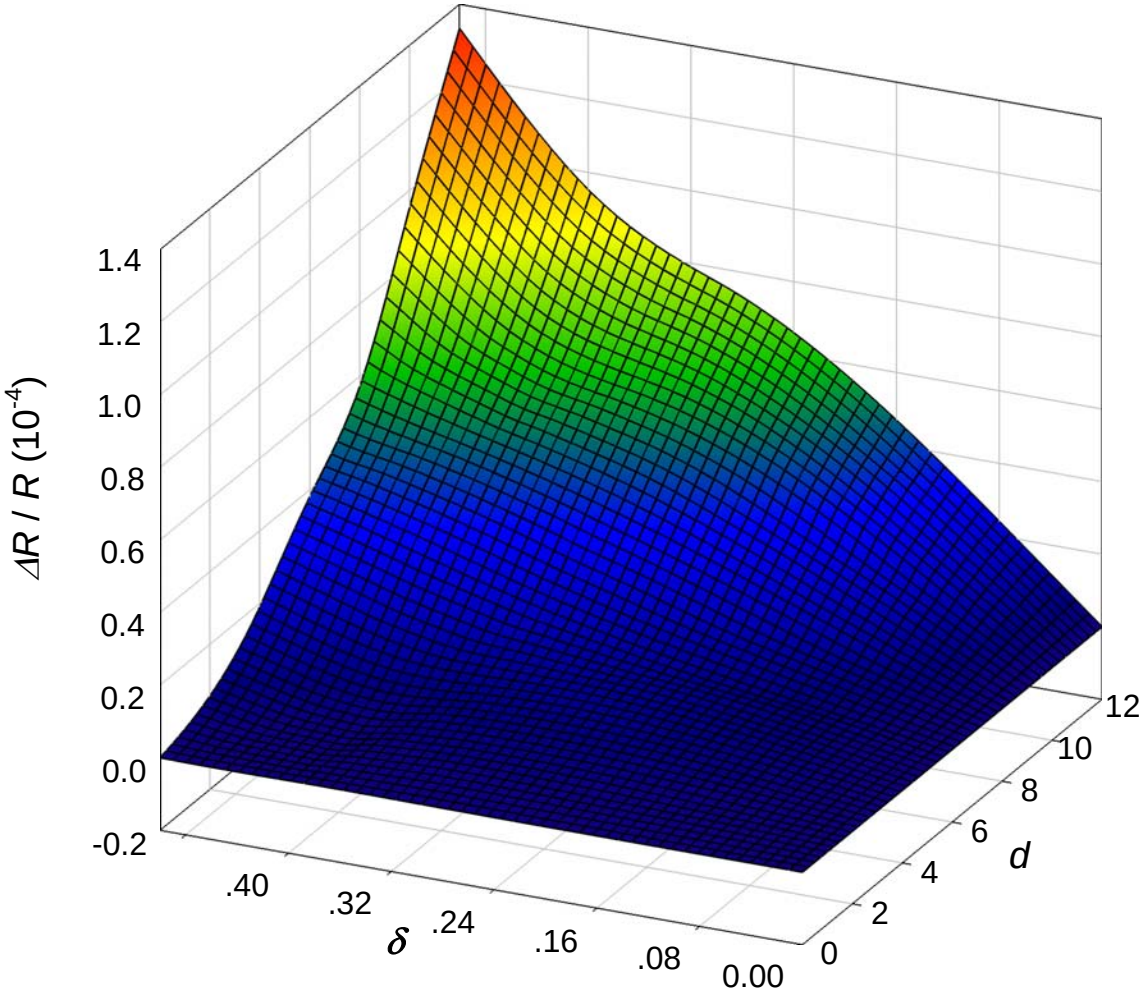

Figure 17. Resistance change of *AD* for various damage size and thickness sets in the size-depth domain.

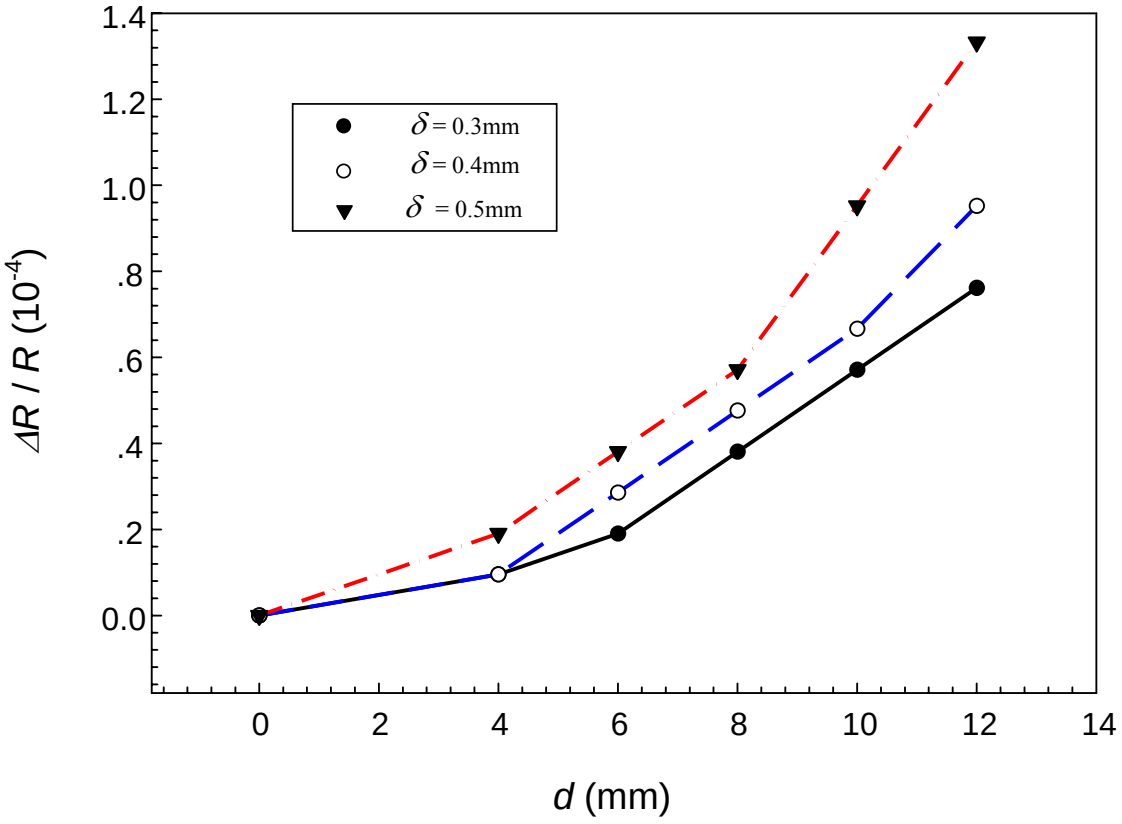

Figure 18. Resistance change for various damage size and thickness sets in the size-thickness domain.

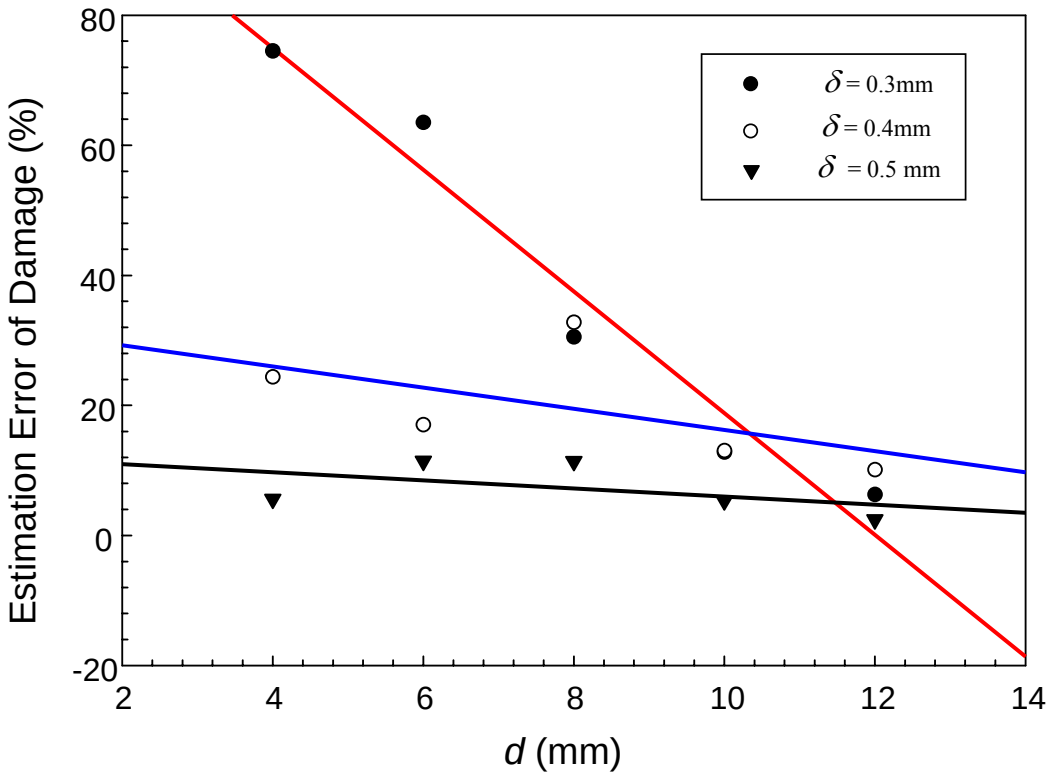

Figure 19. Estimation error of damage for different sets of damage size and depth.

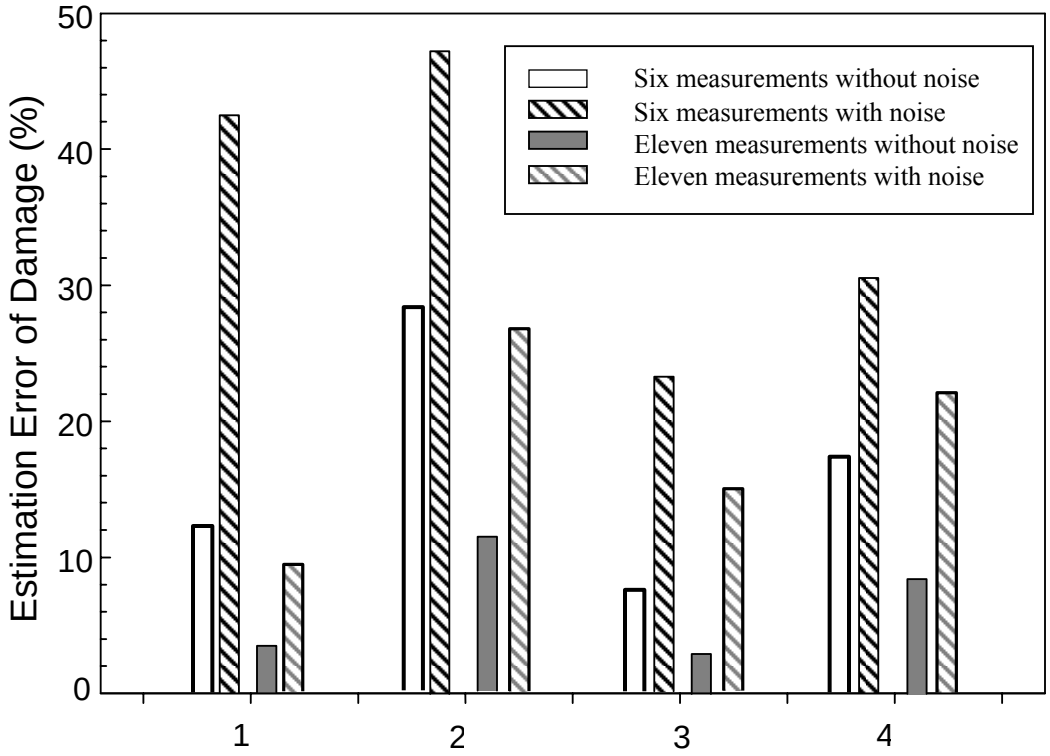

Figure 20. Estimation errors of damage for four cases with different input damages. Both situations with different measurements are listed for comparison and for each situation, error sensitivity is performed.

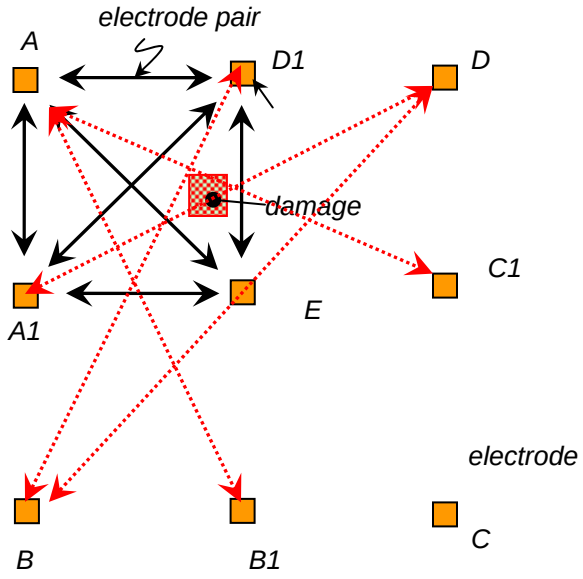

Figure 21. Resistances between electrode pairs used as measurements when doing the inverse analysis. Broken lines implicate the extra five resistances.

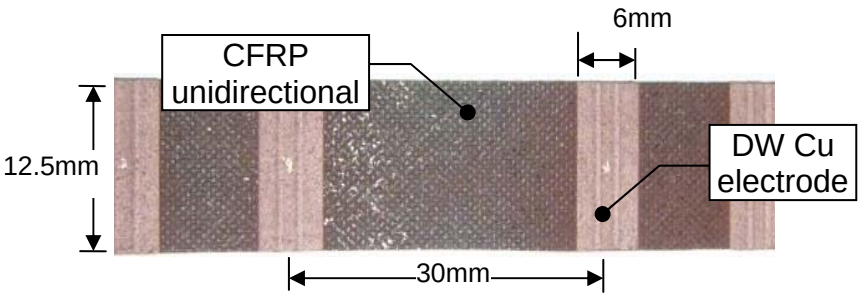

Figure 22. A section of unidirectional fiber reinforced epoxy plate ($t \sim 0.52$mm) with DW electrodes.

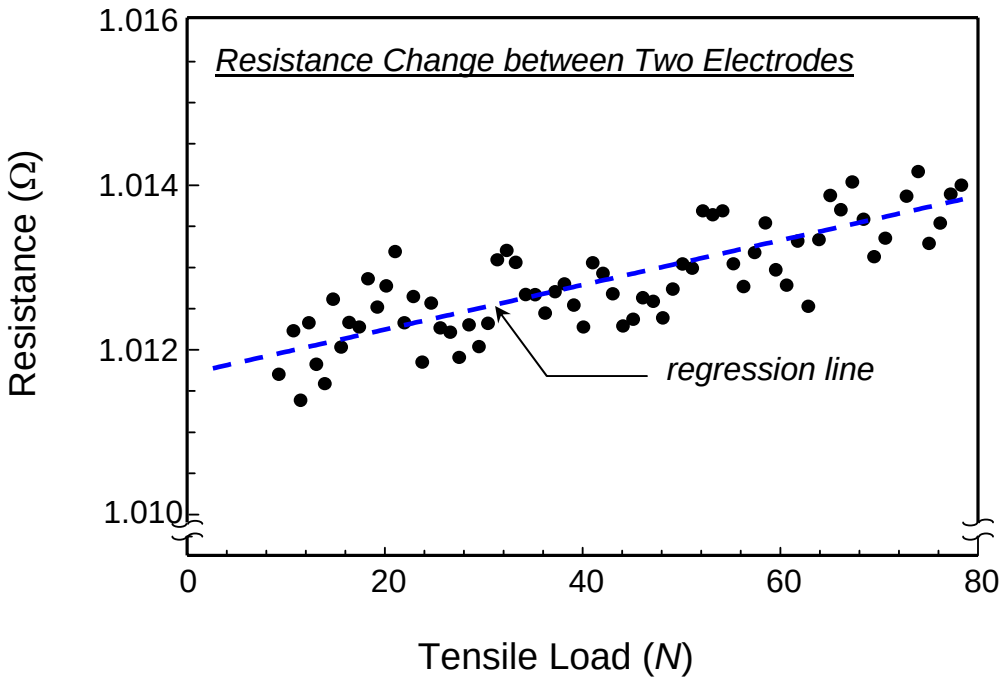

Figure 23. Measured resistance change under tensile load.

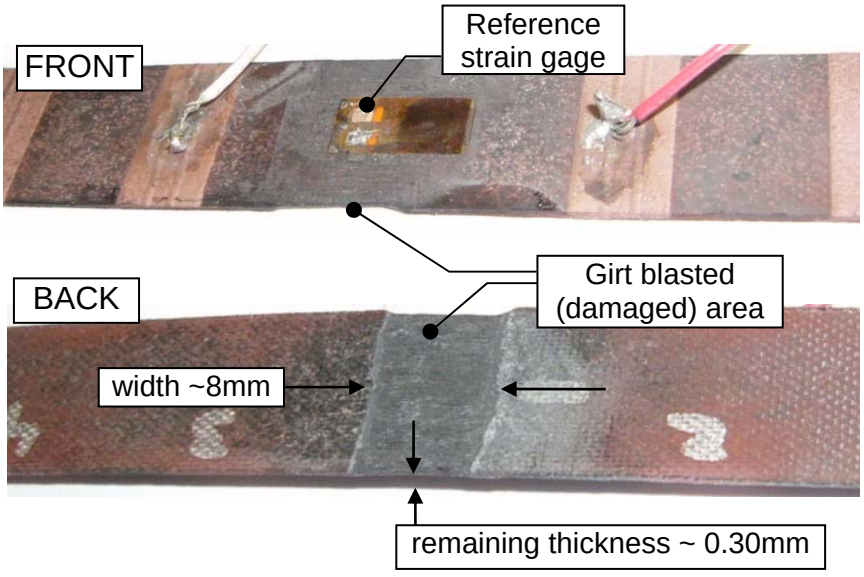

Figure 24. CFRP laminate with artificially imposed damage with grit blasting on back side.

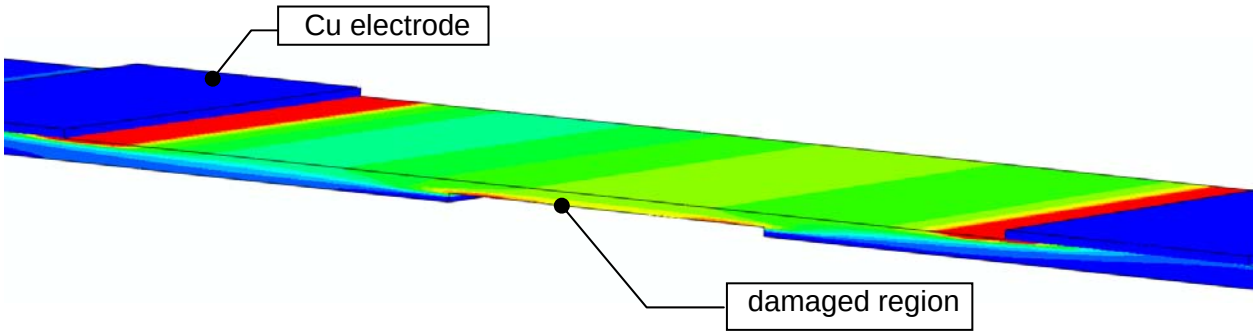

Figure 25. Finite element simulation showing the resistance to electrical flow in damaged laminate.

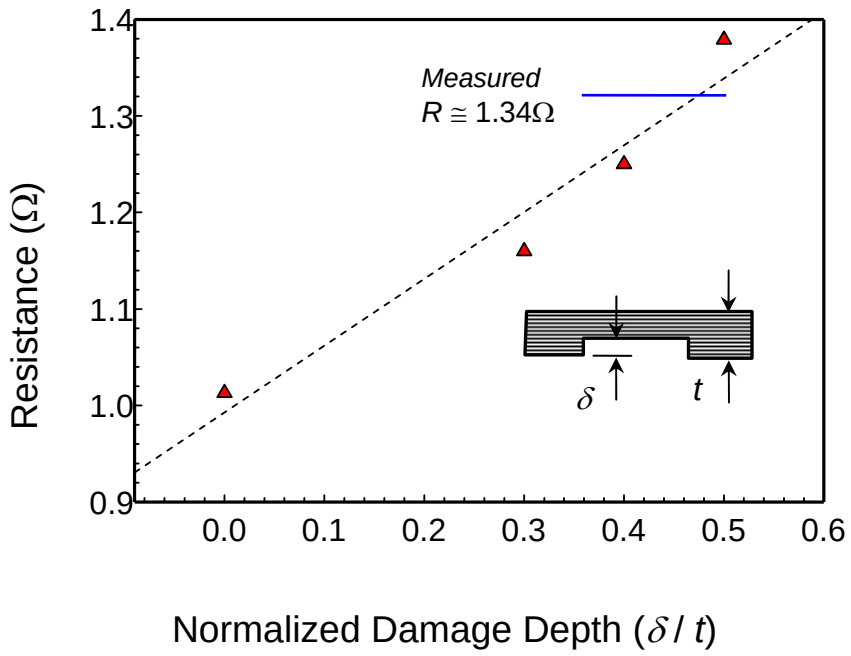

Figure 26. Computed resistances with various damage size/depth. Experimentally measured value is shown for reference.

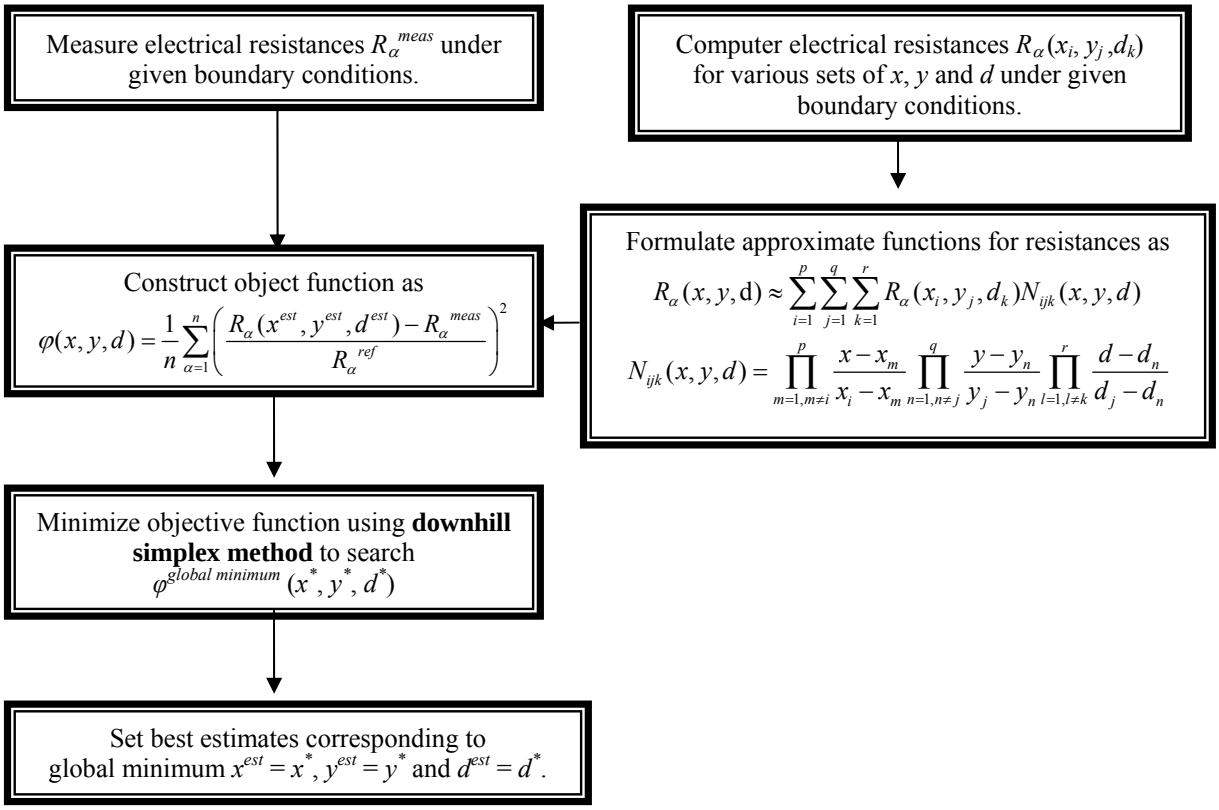

Figure 27. Outline of inverse analysis procedure to estimate unknown parameters.

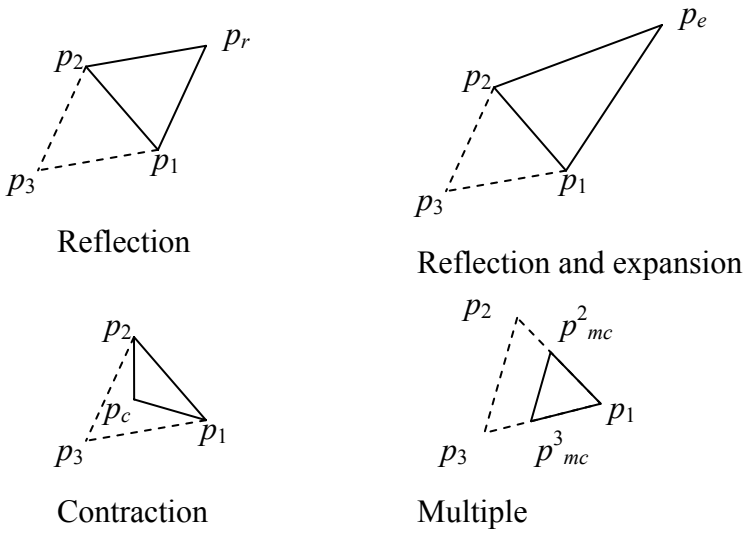

Figure 28. Possible moves of downhill simplex method in the domain of unknown parameters.

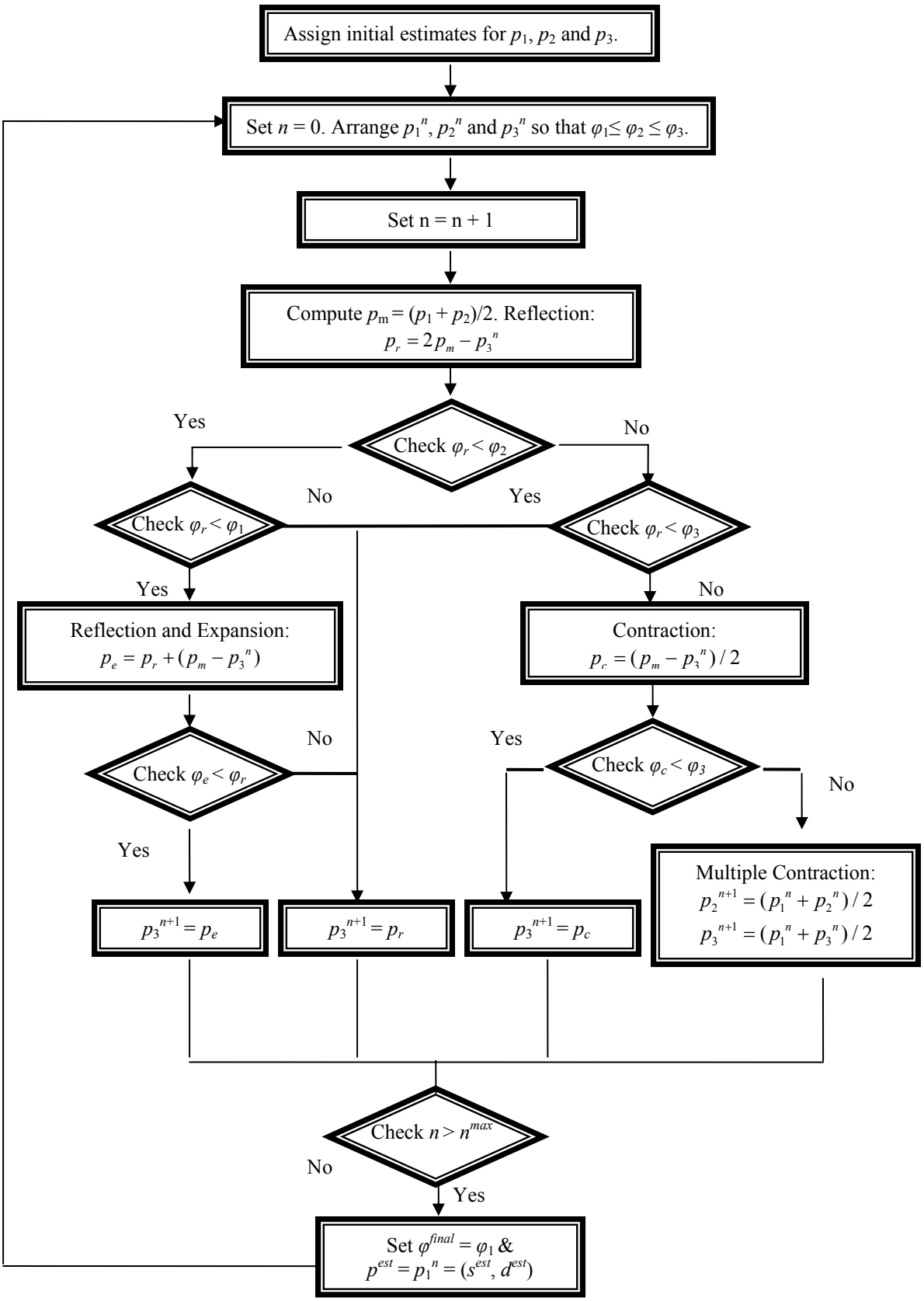

Figure 29. Flow chart for the downhill simplex method.